Penerbit Akademia Baru

Journal of Advanced Research in Fluid Mechanics and Thermal Sciences

Journal homepage: www.akademiabaru.com/arfmts.html
ISSN: 2289-7879

Numerical Simulation of Entropy Generation of Conjugate Heat Transfer in A Porous Cavity with Finite Walls and Localized Heat Source

Ahmed Kadhim Hussein[1], Muhaiman Alawi Mahdi[2], Obai Younis[3,4,*]

[1] College of Engineering, Mechanical Engineering Department, University of Babylon - Babylon City, Hilla, Iraq
[2] Graduated Engineer and Independent Researcher, Babylon City, Hilla, Iraq
[3] College of Engineering at Wadi Addwaser, Mechanical Engineering Department, Prince Sattam Bin Abdulaziz University, Wadi Addwaser, Saudi Arabia
[4] Faculty of Engineering, Department of Mechanical Engineering, University of Khartoum, Khartoum, Sudan

ARTICLE INFO

Article history:
Received 9 February 2021
Received in revised form 10 April 2021
Accepted 13 April 2021
Available online 23 July 2021

Keywords:
Entropy production; Conjugate heat transfer; Free convection; Porous cavity

ABSTRACT

In this research, the entropy production of the conjugate heat transfer in a porous cavity with respect to heat source and solid wall's locations has been studied numerically. Three different cases of the cavity with finite walls thickness and heat source locations are considered in the present study. For both cases one and two, the cavity considered has a vertical finite walls thickness, while the cavity with the horizontal finite walls thickness is considered for case three. For cases one and two, the left sidewall of the cavity is exposed to heat source, whereas the rest of this wall as well as the right sidewall are adiabatic. The upper and lower cavity walls are adiabatic. For case three, the lower wall is exposed to a localized heat source, while the rest of it is assumed adiabatic. The upper wall is cold, whereas the left and right sidewalls are adiabatic. The flow and thermal fields properties along with the entropy production are computed for the modified Rayleigh number ($150 \leq Ra_m \leq 1000$), thermal conductivity ratio ($1 \leq K_r \leq 10$), heat source length ($0.2 \leq B \leq 0.6$), aspect ratio ($0.5 \leq AR \leq 2$) and walls thickness ($0.1 \leq D_1 \leq 0.2$ and $0.1 \leq D_2 \leq 0.2$) respectively. The results show that, the maximum values of the entropy generated from fluid friction develop close to the cavity wall-fluid interfacial, while the maximum values of the entropy generated from heat transfer develop nearby the heat source region. The average Bejan number (Be_{av}) is higher than (0.5) for cases one and two. While for case three, it was found to be less than (0.5). Also, the results show that as the modified Rayleigh number, thermal conductivity ratio, heat source length and aspect ratio increased, the fluid flow intensity in the cavity increased. While, it decreased when the walls thickness increased. From the results, it is concluded that case three gives a higher heat transfer enhancement. The obtained results are compared against another published results and a good agreement is found between them.

---

[*] *Corresponding author.*
E-mail address: oubeytaha@hotmail.com

https://doi.org/10.37934/arfmts.84.2.116151

1. Introduction

Free convection is a fluid motion caused by buoyancy forces that results from the density variations due to variations of temperatures in the fluid. During the past years, the analysis of the thermal fields in the cavity filled with a fluid-saturated porous media received great interest, as it is found in a wide range of engineering applications like solar power collectors, energy drying processes, and pollutants dispersion. Detailed reviews of convection heat transfer applications in a porous media are reported in the recently published books by Pop and Ingham [1], Vafai [2], Ingham and Pop [3] and Nield and Bejan [4]. During the past years, many studies considered the free convection in cavities filled with the porous media [5-12]. Furthermore, the analysis of the joint conduction and free convection heat transfer in a cavity filled with a porous media received great concern by considerable number of investigators as it is widely found in practical applications such as buildings isolation, double-glazing windows, electronic devices cooling and cold storage installations.

Saeid [13,14] numerically explored conjugate free convection in a vertical porous enclosure bounded by finite walls. The authors reported that, the increment in both Rayleigh number and the thermal conductivity ratio resulted in increasing the average Nusselt number. Al-Amiri *et al.,* [15] undertook numerical simulation of the steady conjugate free convection in 2D porous cavity. The reported results suggested that, the Nusselt number was weakly correlated with aspect ratio, whereas it was a strongly correlated with the thermal conductivity ratio (K_r). Saleh and Hashim [16] investigated the influence of wall conduction on the free convection in a square porous cavity being internally heated at a rate directly related to the local temperature difference. It was found that, the maximum fluid temperature increased with increasing thermal conductivity ratio and/or reducing the wall thickness. Chamkha and Ismael [17] presented numerical simulation of the conjugate free convection in a square porous enclosure subjected to internal heating by a solid isosceles triangular domain located at the bottom left corner. They concluded that, the average Nusselt number and fluid flow intensity was increased with Rayleigh number. Alhashash *et al.,* [18] reported the conjugate heat transfer in a square porous cavity with local heating and lateral cooling. The main objective of their study was to determine the influence of bottom wall conduction. The authors deduced that, there is a critical wall thickness for a high wall conductivity below which the increasing wall thickness increases the heat transfer rate and above which the increasing wall thickness decreases the heat transfer.

Entropy production minimization relied upon 2nd law of thermodynamics which states that all process are irreversible processes. The entropy generated in the thermal convection due to the heat transfer and friction losses, and therefore a portion of energy is lost throughout the process because of irreversibility [19]. Varol *et al.,* [20] explored the entropy generated from the conjugate free convection in cavity with vertical solid walls having various thicknesses. They reported that, high Rayleigh numbers enhanced the heat transfer and total entropy generation rate. Kaluri and Basak [21] presented a numerical study about the entropy generated from the free convection in porous square cavities being discretely heated. They found that, at low Darcy and Prandtl numbers, the entropy generated from heat transfer was dominating. In contrast, the fluid friction irreversibility was dominating at high Prandtl and Darcy numbers. Kaluri and Basak [22] investigated the entropy production of laminar free convection flow in porous square cavities with distributed heat sources. The authors reported that, the entropy generated from the heat transfer irreversibility was dominating because of the conduction at low Darcy number. While, the entropy generated from the fluid friction irreversibility was dominating when Darcy number increased. Basak *et al.,* [23] explored the influence of various thermal boundary conditions on entropy production in porous cavity free convection flow. Five different boundary conditions were considered. It was deduced that, the entropy production rates for uniform heating case were higher than that for non-uniform heating cavity. Basak *et al.,* [24] undertook numerical simulation of entropy production in free convection of a porous media confined in a tilted square cavity. The authors reported that, maximum heat transfer and minimum entropy production occurred for ($\Phi \leq 30°$) cavities at high Darcy number (i.e., Da = 10^{-3}) and low Prandtl number (i.e., Pr = 0.025). Lam and Prakash [25] numerically investigated the free convection and entropy production in a porous cavity with heat sources. The authors concluded that, when the conduction was dominating, the entropy production in the cavity was dominated by the heat transfer irreversibility and high Bejan number, while the entropy production was dominated by the fluid friction irreversibility when the convection was dominant. Basak *et al.,* [26] explored the entropy production of conjugate free convection in a square cavity with different wall thickness. The authors noticed that, the maximum entropy generated from the heat transfer occurred close to the solid-fluid interfacial, while the maximum value of the entropy generated from the fluid friction occurred in the vicinity of the walls. Zahmatkesh [27] investigated the orientation impact on natural convection flow in an oblique porous media. The vertical walls of the cavity were subjected to differential heating, while the horizontal ones were adiabatic. Four inclination angles were considered π/4, 3π/4, 5π/4, and 7π/4. For all studied cases, the author observed that the irreversibility was dominated by fluid friction effects. It was concluded that, cavities with hot top wall and cold bottom walls achieved the best thermal performance according to first and second law of thermodynamics. Japar*et al.,* [28] attempted to minimize the entropy generation in Sinusoidal ribs micro-channel by employing secondary channel geometry. To investigate the impact of cavities, ribs and secondary geometry on entropy generation, the authors compared thermal performance of three different designs of micro channels. Namely, rectangular ribs micro-channel heat sink, sinusoidal cavities micro-channel heat sink and sinusoidal cavities ribs micro-channel heat sink. The performance of this three designed were compared with the convectional design. The authors reported that, entropy generation for all three new designed were less than the conventional one, and hence the new designs are thermally efficient than the convectional one. The best thermal performance was achieved by sinusoidal cavities ribs micro-channel heat sink as it produced the minimum entropy generation. Recently, Armaghani *et al.,* [29] numerically analyzed the entropy generation of Cu – water nanofluid in I- shaped cavity due to MHD natural convection. The top wall of the cavity was maintained at low temperature and a part of the lower wall was exposed to uniform heat flux, the rest of the walls were considered adiabatic. The authors studied the influence of Hartmann number, nanoparticle volumetric fraction, size of heat source, angle and location of magnetic field on entropy generation. They concluded that, exerting an angle for the morganatic field had a favorable influence on the thermal performance of the studied system. Yang *et al.,* [30] analytically analyzed heat transfer and entropy generation of double layer porous media inside a tube. The tube wall was subjected to a constant heat flux. The authors investigated the influence of different parameters (such as, Biot number, Darcy number and conductivity ratio) on heat transfer and entropy generation. They observed that, when Biot number was small, and Darcy number of first layer was smaller than that for second layer, the total entropy generation rate for a tube filled with double layer was less than that for a tube filled with single layer of porous medium. Dutta *et al.,* [31] researched the influence of non-uniform heating on natural convection and entropy generation in a rhombic enclosure filled with a porous medium. Both left and right walls of enclosure were preserved at low temperature, while top and bottom walls were exposed to non-uniform, varying temperature with unequal phase angles. The authors presented their results for a range of Rayleigh number, Darcy number, and phase deviation angles. It was found that, heat transfer contributed significantly in irreversibility, and location of maximum entropy strongly depended on phase angle.

More recently, Lukose and Basak [32] used the finite element method to investigate the impact of container shape on entropy generation of porous medium. The authors considered different nine containers having the same area and identical heating. For all cases, only the bottom wall of the container was subjected to cold temperature, while the rest of the walls are adiabatic. Two different Darcy numbers were considered. It was reported that for low Darcy number, entropy generation due to fluid friction was dominating at the container center, while for high Darcy number, it was dominating all throughout the container. Containers having curved walls were found to be thermally more efficient compared to other containers. Almuhtady *et al.,* [33] explored entropy generation of magneto hydrodynamic convection in tilted trapezoidal cavity subjected to heating by triangular fin and filled by variable porous medium. The working fluid was a mixture between Al_2O_3 – Cu nanoparticles. The authors investigated the influence of inclination angle, volumetric volume fraction, and the variable porous media porosity (varies exponentially with the smallest distance to the closest wall), and permeability (function of nanoparticle size). They concluded that, heat transfer rate was inversely proportional to the inclination angle, and entropy generation due to heat transfer was always dominant near the heated fins for all studied cases. Sheikholeslami *et al.,* [34] attempted to enhance heat transfer of nano-material by modifying the design of a multi helical tape tabulator. The authors mainly investigated the influence of multi helical tape width and inlet flow velocity on thermal characteristics of nanofluid in a tube. It was concluded that, the increment in tape width ratio resulted an increasing entropy generation due to friction by (58.9 %). While, it was reduced by (89.95 %) when the pumping power was augmented and the tape width ratio was 0.098. Sheikholeslami *et al.,* [35] numerically analyzed entropy generation and heat transfer of nanofluid through a solar collector with twisted tapes. The results were presented for a range of turbulator (1 - 4) and Reynolds numbers (400 – 20000). The authors observed that, the usage of twisted tapes enhanced the flow of nanofluid and enhancing heat transfer rates and increasing pressure losses. It was also noticed that, the exergy loss was reduced due to the usage of twisted tapes and nanofluid.

According to the above extensive literature survey, the case of the conjugate free convection with entropy production in a tilted porous cavity with finite walls and a localized heat source is not considered yet. The primary objective of this research is to study the entropy generated from the heat transfer and fluid friction for three different cases of tilted porous cavity depending on the positions of the heat source and solid walls. Also, suggesting the optimum position of the heat source and the thickness of finite solid walls to improve heat transfer and minimize entropy production.

2. Mathematical Modelling

2.1 Governing Equations and Geometrical Configuration for The Three Study Cases

The current paper considered three different cases of the cavity depending on the locations of the heat source and solid walls. For both cases one and two, the cavity considered has a vertical finite walls thickness, while the cavity with a horizontal finite walls thickness is considered for case three. For both cases one and two, the left sidewall of the cavity is exposed to heat source, whereas the rest of the wall is adiabatic. The right sidewall is cold and the other walls are adiabatic. For case three, the lower wall is exposed to a localized heat source, while the other sections of the same wall are adiabatic. The upper wall is cold, whereas the other walls are assumed adiabatic. The cavity is filled with a fluid-saturated porous media. The cavities are of height (H), width (W) (i.e., AR=H/W) and tilted at an angle (Φ) as presented in Figure 1(a) to Figure1(c) respectively. It was assumed that, all thermo-physical properties of the working fluid are constant, excluding the density that follows the Boussinesq approximation. Another important assumption is that a local thermal equilibrium between the porous media and the fluid is assumed.

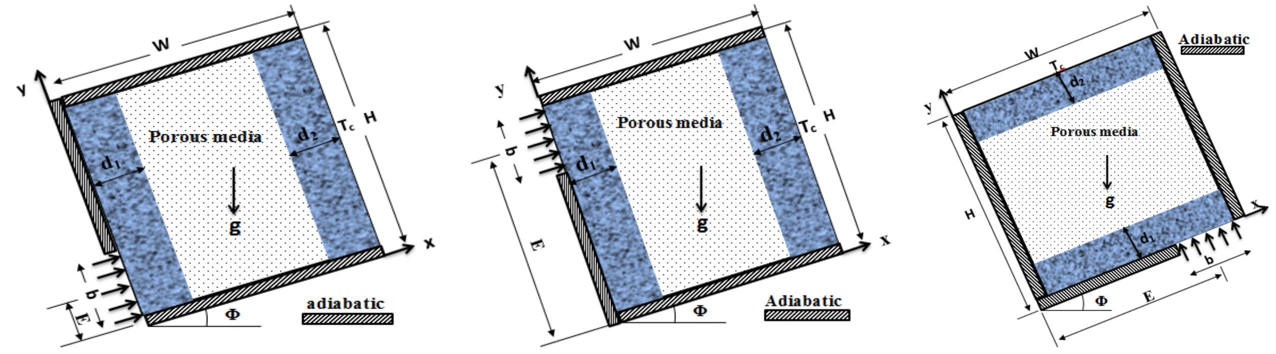

(a) (b) (c)

Fig. 1. Computational domains and coordinate system, (a) Case one, (b) Case two, (c) Case three

The non-dimensional continuity, momentum, and energy equations read [36]

$$\frac{\partial U}{\partial X}+\frac{\partial V}{\partial Y}=0 \tag{1}$$

$$\left(\frac{\partial^2\Psi}{\partial X^2}+\frac{\partial^2\Psi}{\partial Y^2}\right)=Ra_m\left(\frac{\partial\theta_f}{\partial Y}\cos\Phi-\frac{\partial\theta_f}{\partial X}\sin\Phi\right) \tag{2}$$

$$\frac{\partial\Psi}{\partial Y}\frac{\partial\theta_f}{\partial X}-\frac{\partial\Psi}{\partial X}\frac{\partial\theta_f}{\partial Y}=\left(\frac{\partial^2\theta_f}{\partial X^2}+\frac{\partial^2\theta_f}{\partial Y^2}\right) \tag{3}$$

$$\frac{\partial^2\theta_s}{\partial X^2}+\frac{\partial^2\theta_s}{\partial Y^2}=0 \tag{4}$$

These dimensionless parameters are defined as:

$$B=\frac{b}{W},\ Da=\frac{K}{H^2},\ E=\frac{e}{W},\ K_r=\frac{k_s}{k_f}\ \ \mathrm{Ra_m}=\frac{\beta gK(T_h-T_c)W}{\alpha_e\nu_f}$$

$$X=\frac{x}{W},\ Y=\frac{y}{H},\ D=\frac{d}{W},\ \theta_f=\frac{T_f-T_c}{\Delta T},\ \theta_s=\frac{T_s-T_c}{\Delta T},\ \Psi=\frac{\psi}{\alpha_e}\quad \text{and}\quad \Delta T=\frac{q''H}{k_s}$$

2.2 Boundary Conditions

(A) Cases one and two:

The non-dimensional boundary conditions for cases one and two read:

i. The right tilted sidewall is preserved at a constant cold temperature.

at $X=1$ and $0\le Y\le 1\ \theta_s=0,\ \Psi=0$ (5)

ii. For case one, the heat source is localized at the bottom section of the left tilted sidewall of the cavity, whereas the remaining part is considered adiabatic.

at $X = 0$ and $0 \le Y \le B \; q'' = \frac{\partial \theta_s}{\partial X} = -1, \; \Psi = 0$ (6)

at $X = 0$ and $\mathrm{B} < \mathrm{Y} \le 1, \; \frac{\partial \theta_s}{\partial X} = 0, \; \Psi = 0$ (7)

iii. For case two, the heat source is localized at the upper portion of the left tilted sidewall of the cavity, whereas the remaining part is assumed adiabatic.

for $X = 0$ and $0 \le Y < (E - 0.5B), \; \frac{\partial \theta_s}{\partial X} = 0, \; \Psi = 0$ (8)

for $X = 0$ and $(E - 0.5B) \le Y \le 1, \; q'' = \frac{\partial \theta_s}{\partial X} = -1, \; \Psi = 0$ (9)

iv. Lower and upper walls of the cavity are considered adiabatic.

at $Y = 0,1$ and $\begin{bmatrix} 0 \le \mathrm{X} < \mathrm{D}_1 \\ (1\text{-}\mathrm{D}_2) < \mathrm{X} \le 1 \end{bmatrix}, \; \frac{\partial \theta_s}{\partial Y} = 0, \; \Psi = 0$ (10)

at $Y = 0,1$ and $\mathrm{D}_1 \le \mathrm{X} \le (1\text{-}\mathrm{D}_2), \; \frac{\partial \theta_f}{\partial Y} = 0, \; \Psi = 0$ (11)

v. At the interface lines, the following boundary condition is used

$\theta_s = \theta_f, \; \frac{\partial \theta_f}{\partial X} = K_r \frac{\partial \theta_s}{\partial X}$ for $\mathrm{X} = \mathrm{D}_1, \mathrm{X} = 1\text{-}\mathrm{D}_2$ and $0 \le Y \le 1$ (12)

(B) Case three:

The non-dimensional boundary conditions for this case read

i. The upper wall is preserved at a constant cold temperature.

at $Y = 1$ and $0 \le X \le 1 \; \theta_s = 0, \; \Psi = 0$ (13)

ii. The heat source locates at the right section of the lower wall.

at $Y = 0$ and $(\mathrm{E}\text{-}\,0.5\mathrm{B}) < \mathrm{X} \le 1, \; q'' = \frac{\partial \theta_s}{\partial Y} = -1, \; \Psi = 0$ (14)

iii. The other parts of the lower wall are assumed adiabatic.

at $Y = 0$ and $0 \le X \le (E - 0.5B)$, $\frac{\partial \theta_s}{\partial Y} = 0, \ \Psi = 0$ (15)

iv. Left and right tilted sidewalls are adiabatic, i.e.,

at $X = 0,1$ and $\begin{cases} 0 \le \mathrm{Y} < \mathrm{D}_1 \\ (1 - \mathrm{D}_2) < \mathrm{Y} \le 1 \end{cases}$, $\frac{\partial \theta_s}{\partial X} = 0, \ \Psi = 0$ (16)

at $X = 0,1$ and $\mathrm{D}_1 \le \mathrm{Y} \le (1\text{-}\mathrm{D}_2)$, $\frac{\partial \theta_f}{\partial X} = 0, \ \Psi = 0$ (17)

v. At the interface lines, the following boundary condition is used

$$\theta_s = \theta_f \ , \ \frac{\partial \theta_f}{\partial Y} = K_r \frac{\partial \theta_s}{\partial Y} \text{ at } Y = D_1, Y = 1 - D_2 \text{ and } 0 \le X \le 1 \tag{18}$$

2.3 Local and average Nusselt numbers

The local and average Nusselt numbers of the fluid for both cases one and two can be written as

$$Nu_f = \left(-\frac{\partial \theta_f}{\partial X}\right)_{X = D_1, 1 - D_2} \ , \ \overline{Nu_f} = \int_0^1 Nu_f \, dY \tag{19}$$

The local and average Nusselt numbers of the solid wall for case one can be written as

$$Nu_s = \left(\frac{1}{\theta_s}\right)_{X = 0} \ , \qquad \overline{Nu_s} = \frac{1}{B} \int_0^B Nu_s \, dY \tag{20}$$

The local and average Nusselt numbers of the solid wall for case two can be written as

$$Nu_s = \left(\frac{1}{\theta_s}\right)_{X = 0} \ , \qquad \overline{Nu_s} = \frac{1}{B} \int_{E - 0.5B}^{1} Nu_s \, dY \tag{21}$$

While, for case three, the local and average Nusselt numbers of the fluid phase at the interface regions can be written as

$$Nu_f = \left(-\frac{\partial \theta_f}{\partial Y}\right)_{Y = D_1, 1 - D_2} \ , \ \overline{Nu_f} = \int_0^1 Nu_f \, dX \tag{21}$$

And the local and average Nusselt numbers of the solid wall for case three can be written as

$$Nu_S = \left(\frac{1}{\theta_S} \right)_{Y=0}, \overline{Nu_S} = \frac{1}{B} \int_{E-0.5B}^{1} Nu_S dX \tag{23}$$

2.4 Entropy Generation

2.4.1 Entropy generated from the heat transfer

The non-dimensional local entropy generated from the heat transfer in the solid and fluid phases read [36]:

$$S_\theta^s = K_r \left[\left(\frac{\partial \theta_S}{\partial X} \right)^2 + \left(\frac{\partial \theta_S}{\partial Y} \right)^2 \right] \tag{24}$$

$$S_\theta^f = \left[\left(\frac{\partial \theta_f}{\partial X} \right)^2 + \left(\frac{\partial \theta_f}{\partial Y} \right)^2 \right] \tag{25}$$

The local entropy generated from the heat transfer is obtained by adding both the local entropy generated from heat transfer in the solid wall and fluid phases.

$$S_\theta = S_\theta^s + S_\theta^f \tag{26}$$

2.4.2 Entropy generated from the fluid friction

The local entropy generated from fluid friction irreversibility in the fluid phase is defined as [20]:

$$S_\Psi^f = \phi \left[4 \left(\frac{\partial^2 \Psi}{\partial X . \partial Y} \right)^2 \right] \tag{27}$$

Where, $\left(S_\Psi^f \right)$ is the local entropy generated from fluid friction in the fluid phase and (ϕ) is called irreversibility distribution ratio that is defined by Basak *et al.*,[26]

$$\phi = \frac{\mu_f T_f}{k_f} \left(\frac{\alpha_e}{W (\Delta T)} \right)^2 \tag{28}$$

In the present work, $\left(S_\Psi^f \right)$ is calculated by using Eq. (27) and ($\phi = 10^{-3}$) [21,28].

2.4.3 Total entropy generation and the average Bejan number

The total entropy generation (S_{tot}) is obtained by adding the local entropy generated from the heat transfer to that generated from fluid friction:

$$S_{tot} = S_{\theta} + S_{\Psi}^{f} \tag{29}$$

The global total entropy generated from heat transfer and fluid friction is calculated by the integration of local entropy production rates (S_{θ}) and $\left(S_{\Psi}^{f}\right)$ over the domain Ω .

$$S_{\theta,tot} = \int_{\Omega} S_{\theta} d\Omega \tag{30}$$

$$S_{\Psi,tot} = \int_{\Omega} S_{\Psi}^{f} d\Omega \tag{31}$$

The global total entropy generation reads

$$S_{tot,\Omega} = S_{\theta,tot} + S_{\Psi,tot} \tag{32}$$

While, the average Bejan number (Be_{av}) reads [36]

$$Be_{av} = \frac{S_{\theta,tot}}{S_{tot,\Omega}} \tag{33}$$

3. Discussion of Results

3.1 Numerical Solution, Mesh Dependence Study and Method Validation

The numerical solution was performed based on the Finite Difference Method (FDM) [37] and by using an in-house personal code, completely developed by the authors. Uniform mesh distributions are utilized for the entire cavity. The influence of grid size resolution is tested to adopt the proper grid size as shown in Figure 2. The grid size varies from (40 × 40) to (200 × 200) and the number of grids that is adopted in the present work is (140 × 140). To validate the mathematical model used in the current study, our results are compared against the results reported by Saeid [14] for streamline and isotherm contours at [Φ = 0°, Ra_m=1000, K_r= 1 and D_1= D_2= 0.2]. Also, another comparison is obtained for the entropy generated from the fluid friction and heat transfer between the present study results and Zahmatkesh [27] at [Φ = 45°, Ra_m= 100 and R_d= 4]. Both comparisons resulted in a very good agreement as presented in Figure 3 and Figure 4.

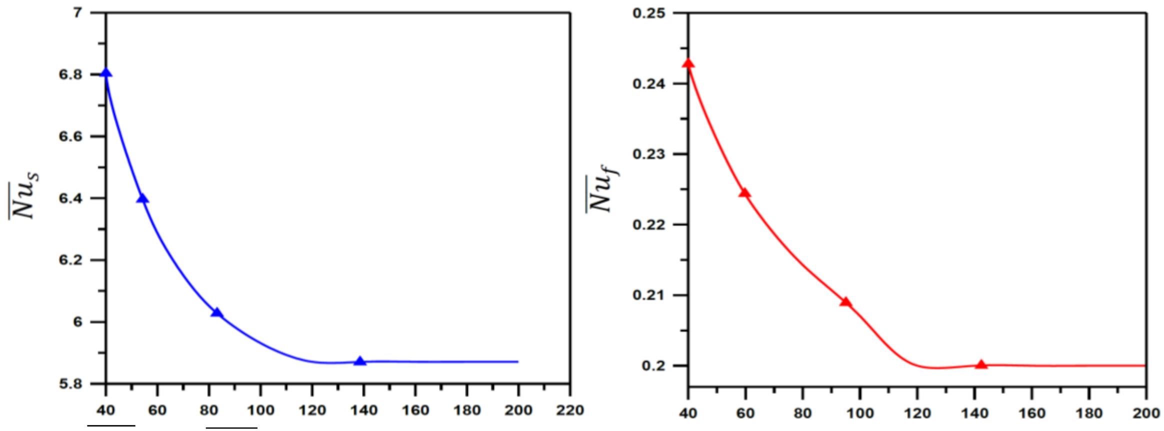

Fig. 2. $\overline{Nu_s}$ and $\overline{Nu_f}$ against number of grid points at [Φ = 30°, Ra$_m$= 1000, K$_r$= 1, B= 0.2, AR= 1 and D$_1$= D$_2$= 0.1]

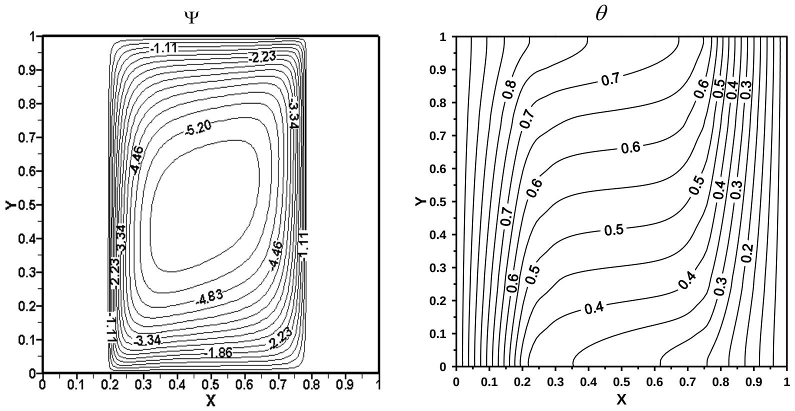

Current study

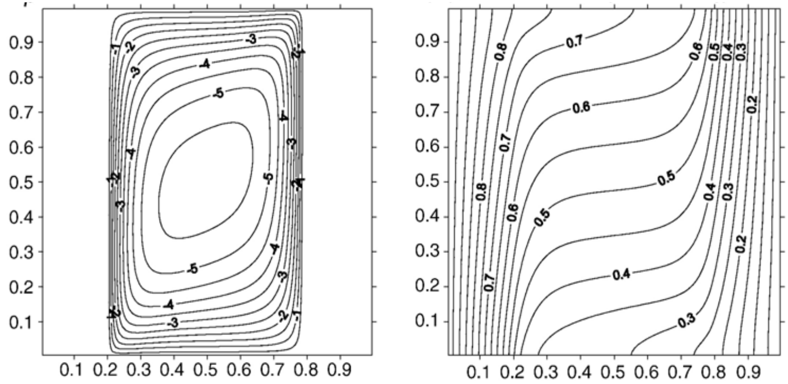

Saeid [14]

Fig. 3. Streamlines (Ψ) and isotherms (θ) contours of the current study and Saeid [14] at [Φ = 0°, Ra$_m$= 1000, K$_r$ = 1 and D$_1$ = D$_2$ = 0.2]

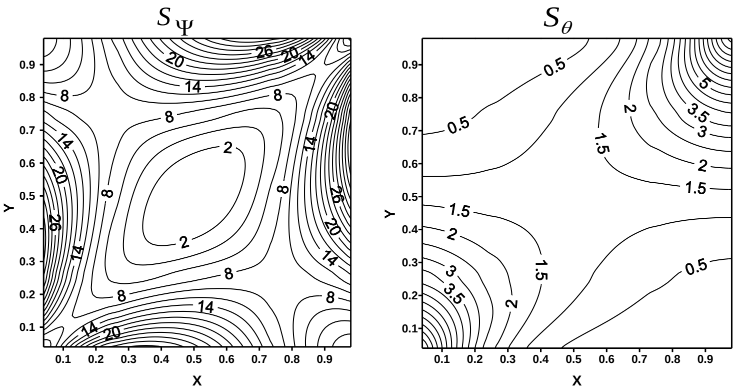

Current study

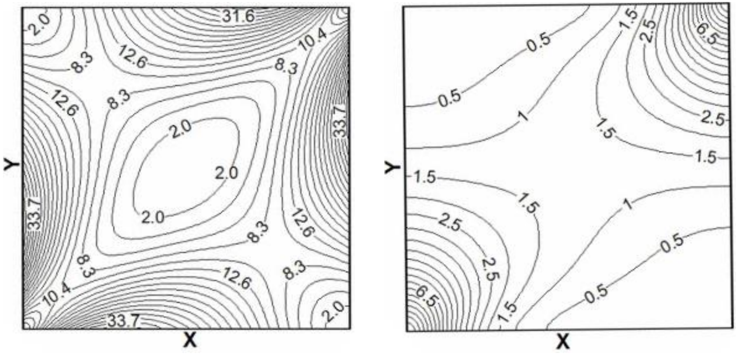

Zahmatkesh [27]

Fig. 4. Comparison of entropy generated from fluid friction and heat transfer between the current study and Zahmatkesh [27] at [Φ = 45°, Ra_m= 100 and R_d = 4]

3.2 Case One

3.2.1 Streamlines, isotherms, and entropy production results

Figure 5 displays streamlines contours (Ψ), isotherms contours (θ) and local entropy generated from fluid friction (S_Ψ) and heat transfer (S_θ) for different modified-Rayleigh numbers and for [Φ = 30°, K_r = 1, B = 0.2, E = 0.1, AR = 1 and D_1 = D_2 = 0.1]. It was noted that, whereas the (Ra_m) increases from (Ra_m = 150) to (Ra_m = 500), the maximum absolute value of the stream function rises from [$|\Psi|_{, max}$ = 1.27] to [$|\Psi|_{, max}$ = 2.88]. This is caused by the increment in the flow circulation strength when the modified-Rayleigh number increased. In fact, for high value of (Ra_m), the effect of both the buoyancy force and free convection in the porous media tend to be very strong which leads to an increment in the stream function values. With regards to isotherms, it is clear that whenever the modified-Rayleigh number is relatively low [Ra_m = 150], the isotherms are in general have a regular shape. This is mainly because of weak influence of the convection as the conduction heat transfer is dominating. However, for relatively high values of modified-Rayleigh number [Ra_m=1000], the isotherms shape is clearly changed, and the convection is dominant.

In regards to the behavior of entropy generated from fluid friction and heat transfer, it was noted that as the modified-Rayleigh number increases from [Ra_m = 150] to [Ra_m = 500], the maximum values of entropy generated from fluid friction increase respectively from [$S_{\Psi, max}$=0.0542] to [$S_{\Psi, max}$=0.331] at the lower section of the left sidewall on the solid wall- fluid interface region. Similar, but with a slight increase in values of (S_Ψ) is noticed near the other walls. Again, it may be observed that the effect of (Ra_m) is very weak on (S_Ψ) contours in the center of the cavity. This is due to the minor influence of the friction between the fluid and the walls, as a result the values of (S_Ψ) at this region are reduced. For the entropy generated from heat transfer contours, it was noted that the position of the heat source in the lower section of the left sidewall plays an important role in accumulating (S_θ) contours at this zone. This is caused by the high heat transfer at this region which tends to enhance the values of (S_θ) at this location. For regions that located far from the heat source location, the effect of (S_θ) becomes insignificant due to the weak influence of the heat source which leads to diminish the effect (S_θ). Also, insignificant effect of (S_θ) is observed with the fluid phase and the right sidewall as a result of the low value of temperature gradient.

The flow, thermal fields and the local entropy generated from fluid friction and heat transfer are represented in Figure 6respectively for various values of the aspect ratio and for [$\Phi = 30°$, $K_r = 1$, $Ra_m = 1000$, E = 0.1, B = 0.2 and $D_1 = D_2 = 0.1$]. It was noted that, as the aspect ratio is increased from [AR = 0.5] as shown in Figure 6(a) or when the cavity has a rectangular or a slender shape [i.e., AR < 1] to a shallow one [i.e., AR > 1] as presented in Figure 6(b), the flow circulation increases from [$\left|\Psi\right|_{,max}$ = 2.31] for [AR = 0.5] to [$\left|\Psi\right|_{,max}$ = 6.26] for [AR = 2]. In fact, for relatively small aspect ratio [AR = 0.5], the cavity becomes small and consequently the flow circulation region is reduced. While, for higher values of aspect ratio [AR =2], the cavity size increases which causes to enlarge the region of the flow circulation inside the cavity. Thus, it may be deduced that influence of aspect ratio becomes significant and strong for relatively high values of aspect ratio. So, due to the above reasons, the values of the stream function increase as the aspect ratio increases. With regards to isotherms, it was observed from Figure 6(a)and Figure 6(b)that the isotherm lines become more curved especially at the heat source position when the aspect ratio increases. This indicates a strong thermal field especially at the heat source position. Thus, it is deduced that as the value of aspect ratio increased, the convection effect increased also.

With respect to the entropy generated from fluid friction and heat transfer, it was noticed that the values of (S_Ψ) increase as the aspect ratio increases especially at the lower section of the left sidewall where the heat source is placed. The values of (S_Ψ) increase from [0.228] when [AR = 0.5] to [1.482] when [AR = 2]. This result points out that, (S_Ψ) increases as the aspect ratio increases. Therefore, one can observe a clear increase in the buoyancy and the free convection effects when the aspect ratio increases. This increasing leads to increase the friction phenomena between the flow vortices and the cavity walls and as a result the values of (S_Ψ) increases. Also, it is clear that the contours of (S_Ψ) enlarge close to the parallel verticals walls. Moreover, it may be noticed that (S_θ) contours are highly agglomerated closed to the heat source position. This is a direct result of the high temperature gradient at this location which increases the values of (S_θ). In addition, it is clear from Figure 6(a)and Figure 6(b)that the influence of (S_Ψ) and (S_θ) is absent in the center of the cavity. This indicates that, this region is still maintained at the state of the equilibrium. While, the cavity walls and the region of the heat source exhibit a high irreversibility and a state of the non- equilibrium phenomena is dominating.

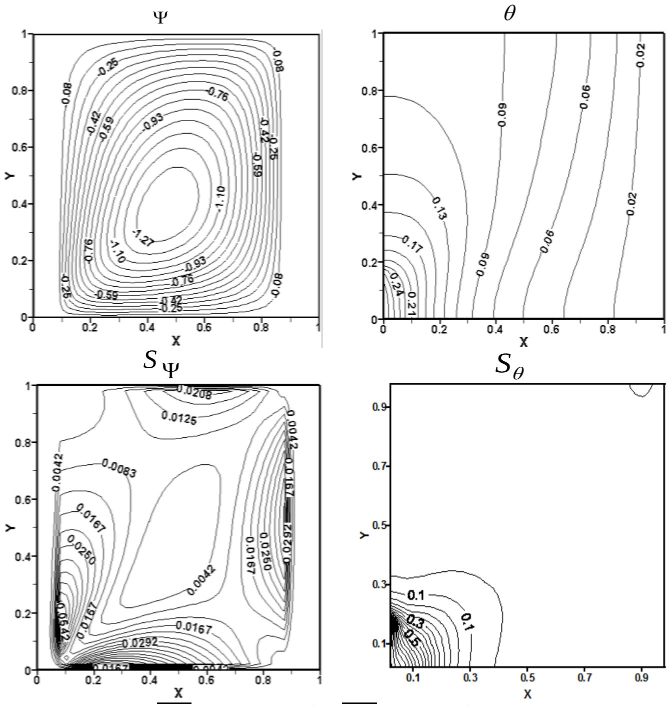

$\overline{Nu_f} = 0.19358, \overline{Nu_s} = 3.65877$

(a) $\mathrm{Ra_m}$ = 150

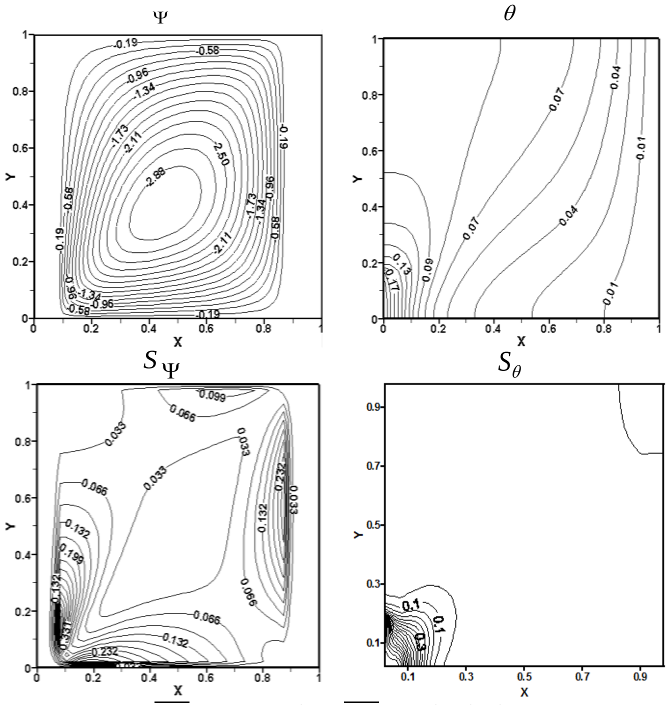

$\overline{Nu_f} = 0.19519, \overline{Nu_s} = 5.05051$

(b) $\mathrm{Ra_m}$ = 500

Fig. 5. Streamlines contours (Ψ), isotherms contours (θ) and local entropy generated from fluid friction (S_Ψ) and heat transfer (S_θ) for various values of ($\mathrm{Ra_m}$) and for [B= 0.2, $D_1 = D_2 = 0.1$, $K_r = 1$, AR = 1, Φ = 30°, E = 0.1]

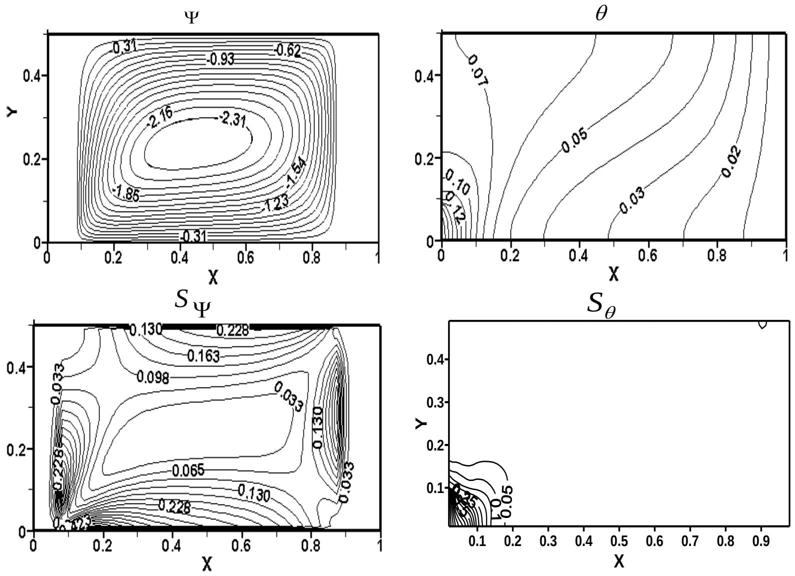

$\overline{Nu}_f = 0.18439, \overline{Nu}_s = 6.31802$

(a) AR= 0.5

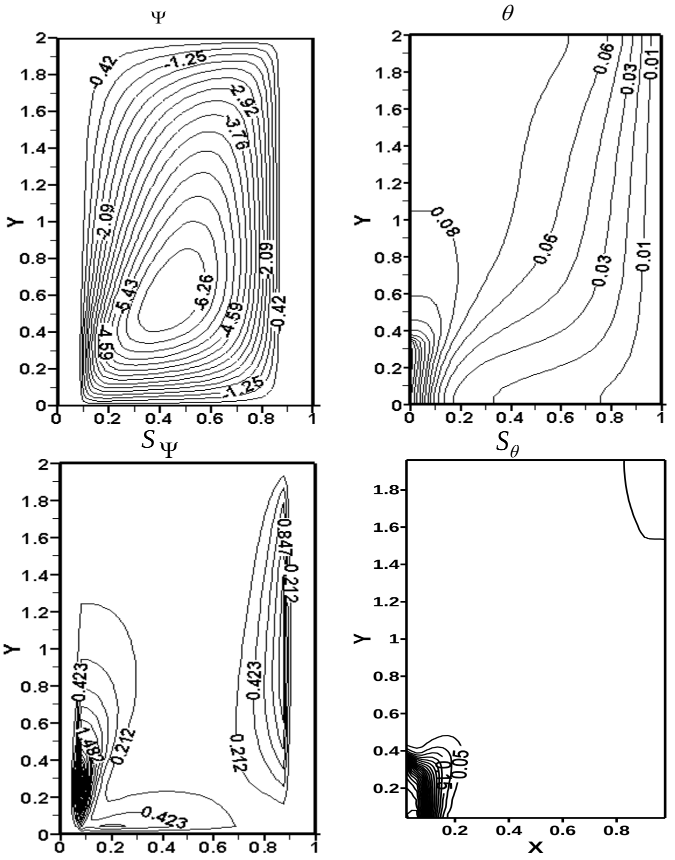

$\overline{Nu}_f = 0.19798, \overline{Nu}_s = 5.65422$

(b) AR = 2

Fig. 6. Streamlines contours (Ψ), isotherms contours (θ) and local entropy generated from fluid friction (S_Ψ) and heat transfer (S_θ) for various aspect ratio and [B= 0.2, $D_1 = D_2 = 0.1$, $K_r = 1$, Ra_m=1000, Φ = 30°, E = 0.1]

Figure 7 illustrates streamlines contours (Ψ), isotherms contours (θ) and local entropy generated from fluid friction (S_Ψ) and heat transfer (S_θ) for various values of walls thickness and [Φ = 30°, AR = 1, Ra_m = 1000, E = 0.1, B = 0.2 and K_r = 1]. The conduction was dominating with increasing walls thickness. From these figures, it may be noticed that the intensity of the fluid flow is reduced with higher walls thickness because of the reduction in the convection heat transfer.Note that, [$|\Psi|_{,\max}$ = 3.89 and 3.49] for cases [$D_1 = D_2$ = 0.15 and 0.2] respectively. From these figures, it was noted that, the core of the vortices starts to shrinkage as the non-dimensional walls thickness is increased. This is a direct result of the domination of the conduction with the increase of the solid walls thickness. From the above, it may be concluded that, the fluid circulation intensity is much higher for a thin solid wall. For the isotherms contours, it was observed that when the thickness of walls is increased, the isotherms pattern becomes more regular. This indicates that the influence of conduction heat transfer becomes more significant. Furthermore, the isotherms pattern indicates that the heat is transferred from the left sidewall where the heat source exists to the cold right sidewall due to the temperature difference, which satisfies the assigned boundary conditions.

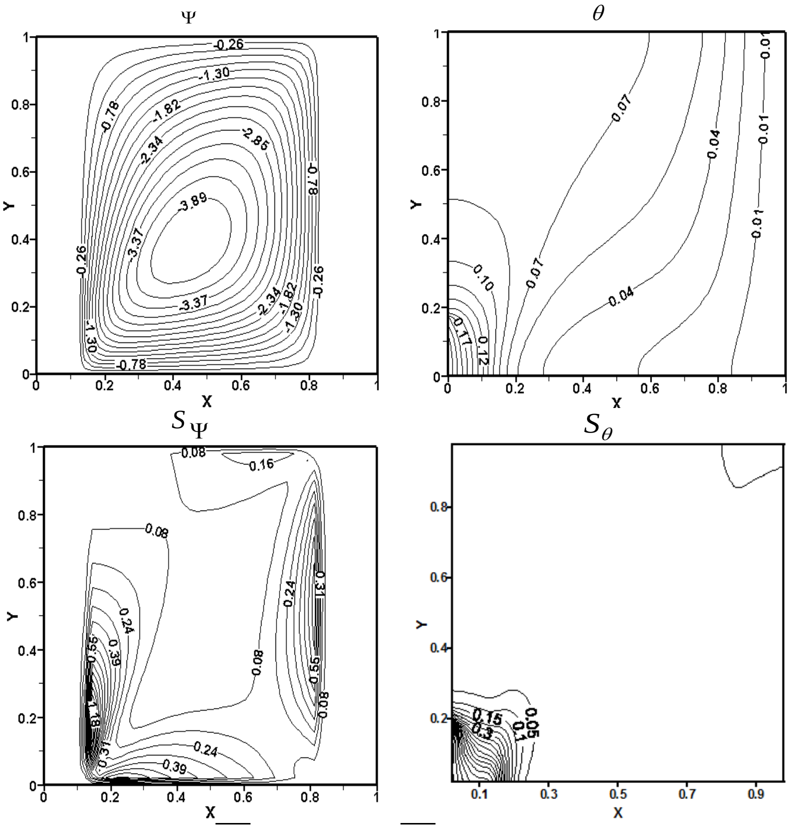

$$\overline{Nu_f} = 0.19220, \overline{Nu_s} = 5.17989$$

(a) $D_1 = D_2 = 0.15$

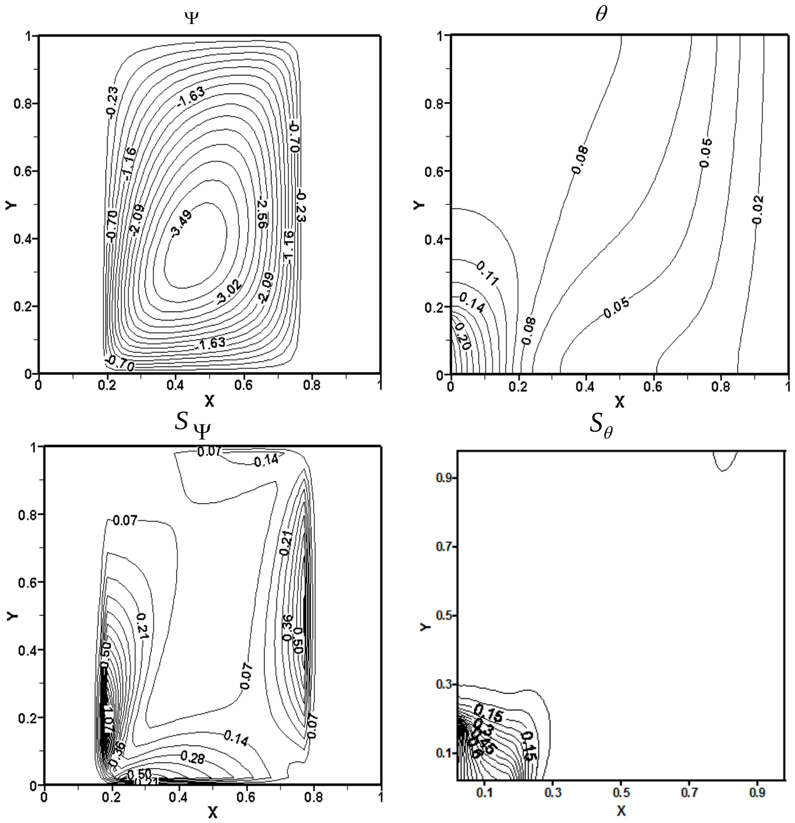

$\overline{Nu}_f = 0.19019, \overline{Nu}_s = 4.39328$

(b) $D_1 = D_2 = 0.2$

Fig. 7. Streamlines contours (Ψ), isotherms contours (θ) and local entropy generated from fluid friction (S_Ψ) and heat transfer (S_θ) for various non-dimensional walls thickness and [B= 0.2, AR=1, K_r = 1, Ra_m=1000, Φ = 30°, E = 0.1]

With respect to the entropy generated from fluid friction and heat transfer, it was noticed that with increasing walls thickness, the convection and the fluid vortices decrease and due to this decreasing, the friction between the fluid vortices and the walls is weakened. This results in decreasing (S_Ψ) as walls thickness increases. From these figures, it can be seen that, at the left wall-fluid interface, the maximum magnitude of (S_Ψ) equals to [1.18] and [1.07] for cases [D1 = D_2 = 0.15 and 0.2] respectively. Another active region of (S_Ψ) are at the bottom and right walls, but with lower values when compared with the left wall-fluid interface. Weak effect of the friction is noted at the upper part of the cavity because of lower velocity gradients. Also, insignificant effect of (S_Ψ) is noticed at the cavity center for all values of walls thickness due to slight effect of friction between the fluid molecules. It was noticed also that, as the wall thickness increases, the entropy generated from heat transfer becomes more uniform in the lower part of the left sidewall where the heat source locates. Insignificant effect of (S_θ) was observed with the other regions of the cavity due to the low thermal gradients.

3.2.2 Local Nusselt number results

The local Nusselt number contours along the heat source (Nu_s) and with the fluid phase (Nu_f) are displayed in Figure 8 for different values of (Ra_m) and [B = 0.2, E = 0.1, K_r=1, D_1= D_2 = 0.1, AR=1 and Φ = 30°]. As expected, the values of both (Nu_s) and (Nu_f) increase as (Ra_m) increases. This is caused by the influence of the buoyancy force and the free convection which are magnified due to the increment in (Ra_m) values from [Ra_m =150] to [Ra_m =500]. Thus, it may be deduced that the heat transfer rates from the heat source and the fluid inside the cavity are increased when the (Ra_m) increased. Figure 8 shows also that, the (Nu_f) at the lower part of the left sidewall is directly proportional to (Ra_m). Whereas, a completely opposite behavior is noticed at the other parts of the left sidewall. This is because of the increment in the convection heat transfer that clearly enhanced the rates of heat transfer.

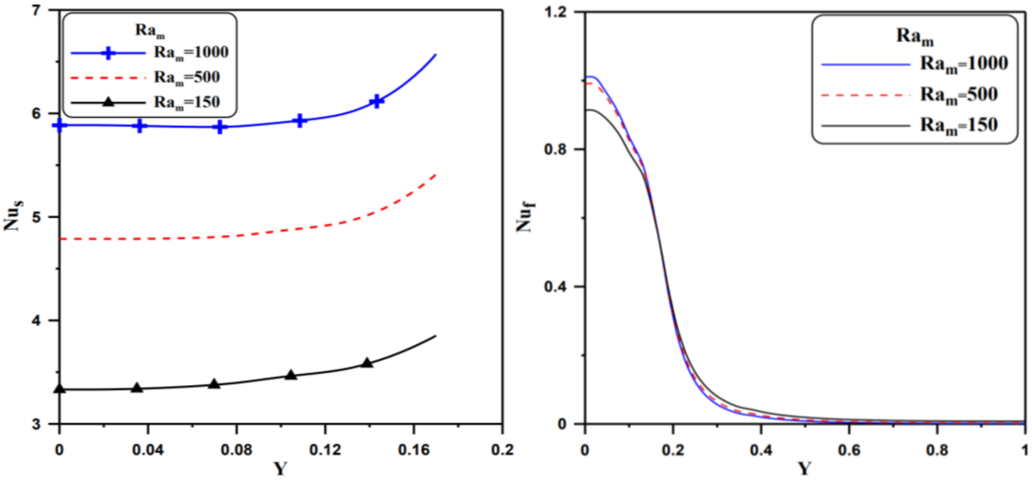

Nu_s Nu_f

Fig. 8. Profiles of (Nu_s) and (Nu_f) for various values of (Ra_m) and [B= 0.2, AR= 1, Φ= 30°, K_r= 1, D_1= D_2= 0.1 and E= 0.1]

Figure 9 illustrates the profiles of (Nu_s) and (Nu_f) for various aspect ratios (AR) and for [B = 0.2, E= 0.1, Ra_m = 1000, K_r = 1, D_1= D_2 = 0.1 and Φ = 30°]. It may be noticed that, when the value of aspect ratio increased form [AR = 0.5] to [AR= 2], the (Nu_s) values increase at the first part of the heat source; while a reverse behavior is observed at the other part. For the behavior of (Nu_f), it can be noted that, it is directly proportional to the aspect ratio. This is caused by the enhancement of the flow circulation intensity inside the cavity when the aspect ratio increased which consequentially resulted in enhancing the convection and as a result, the (Nu_f) values increased. Figure 10 shows (Nu_s) and (Nu_f) profiles for different non-dimensional wall thickness and for [B = 0.2, E = 0.1, Ra_m = 1000, K_r = 1, AR=1 and Φ = 30°]. It was noted that, as the dimensionless wall thickness increases from [D_1= D_2= 0.15] to [D_1= D_2= 0.2], the (Nu_s) begins to decrease. This is because of the significant impact of the conduction heat transfer when values of walls thickness increase which results in decreasing (Nu_s) values. With respect to the profiles of (Nu_f), it can be seen that, they decrease again at the lower section of the left sidewall as values of walls thickness increase. Whereas, an opposite behavior is evident at the middle region of the left sidewall. The main reason of the latter behavior is the increment in the temperature difference between the cold wall and the interface temperature, which leads to decrease (Nu_f) values at the middle region of this wall.

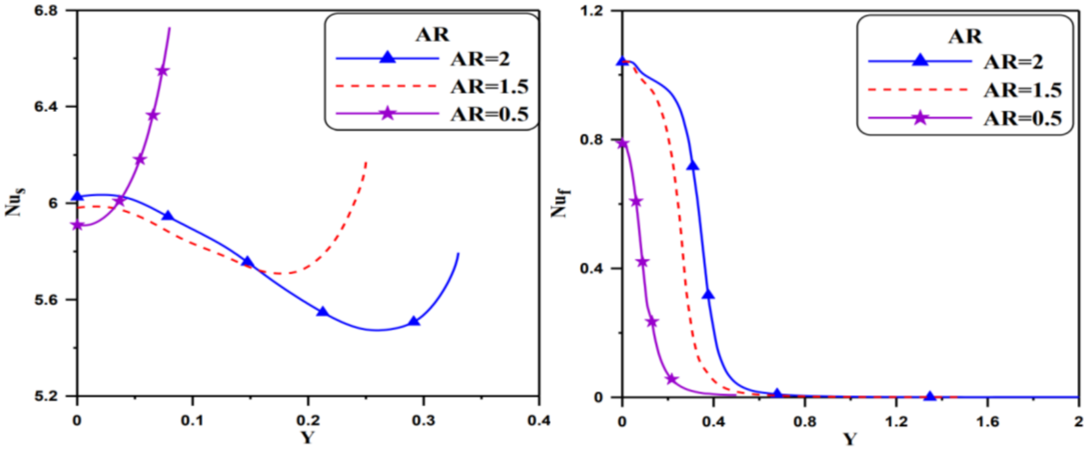

Nu_s Nu_f

Fig. 9. Profiles of (Nu_s) and (Nu_f) for various values of the aspect ratio (AR) and for [B= 0.2, Ra_m= 1000, Φ= 30°, K_r= 1, D_1= D_2 = 0.1 and E= 0.1]

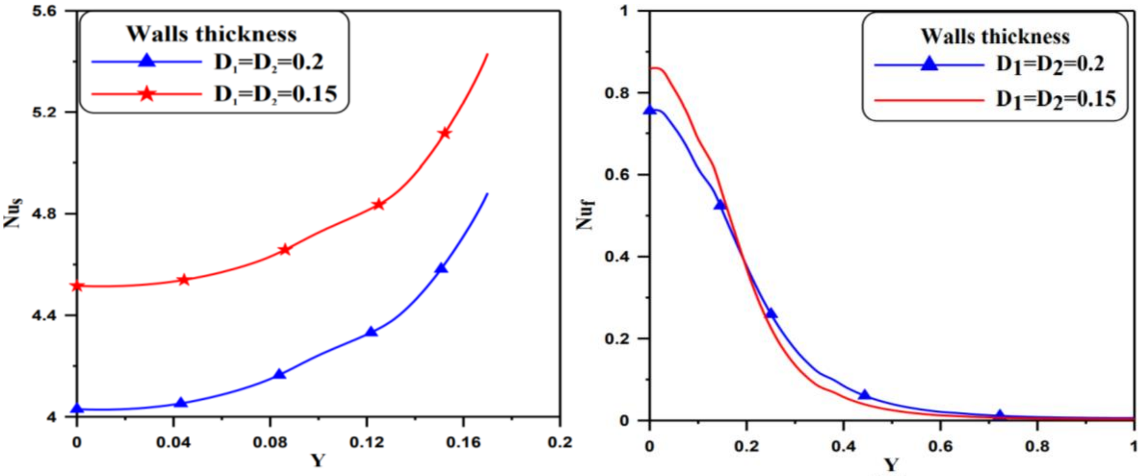

Nu_s Nu_f

Fig. 10. Profiles of (Nu_s) and (Nu_f) for various values of walls thickness and for [B= 0.2, AR= 1, Φ = 30°, K_r= 1, Ra_m= 1000 and E = 0.1]

3.2.3 Average Nusselt number results

The results suggest that, ($\overline{Nu_f}$) increases when (Ra_m and AR) increase, while a reverse behavior of it is observed when the walls thickness increases. For the behavior of the ($\overline{Nu_s}$), it may be observed that it is directly proportional to (Ra_m), while a reverse behavior of it can be seen with increasing (AR and (D_1 and D_2)).

3.2.4 Average Bejan number results

Figure 11 presents the connection between the average Bejan number (Be_{av}) and the modified Rayleigh number (Ra_m) for various values of the wall thickness. The average Bejan number denotes the dominance of the fluid friction or thermal irreversibility on the total entropy production. When (Be_{av} > 0.5), the entropy generated from heat transfer is dominant, while when (Beav< 0.5), the entropy generated from fluid friction is dominant. The results indicate that, the average Bejan number is in an inverse proportionto (Ra_m). This is connected with the definition of (Be_{av}) which is known as ratio of the entropy generated from the heat transfer to the total entropy production. From this definition, it can be noticed that when (Ra_m) increases, the fluid intensity increases which leads to increase the total entropy production. This due to that the (Be_{av}) decreases. The results show that, (Be_{av}) increases when (D_1) and (D_2) increase. The entropy generated from the heat transfer is dominating in this case. This can be seen from the minimum value of (Be_{av}) which is greater than (0.5) as shown fromFigure 11.

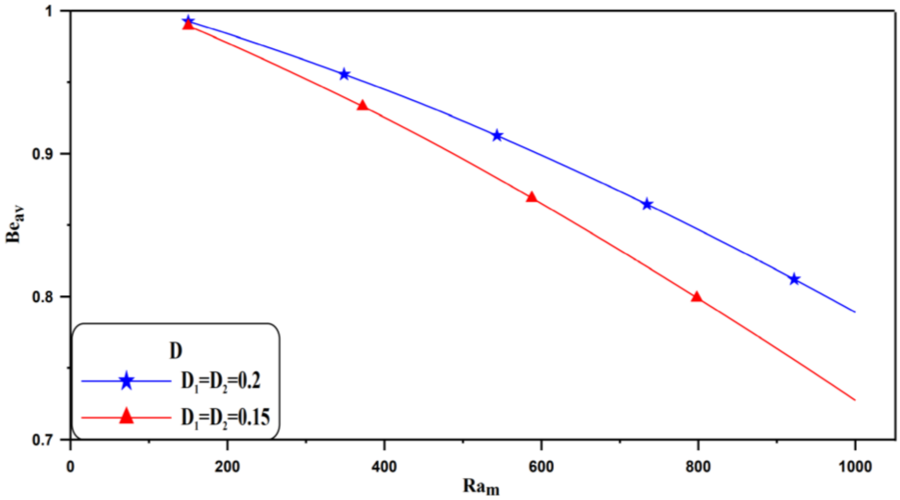

Fig. 11. Average Bejan number (Be_{av}) versus (Ra_m) for various values of walls thickness (D_1 and D_2) and [B = 0.2, AR = 1, Φ = 30°, K_r = 1, Ra_m= 1000 and E= 0.1]

3.3 Case Two

3.3.1 Streamlines, isotherms and entropy production results

Figure 12 displays streamlines contours (Ψ), isotherms contours (θ) and local entropy generated from fluid friction (S_{Ψ}) and heat transfer (S_{θ}) for different modified-Rayleigh numbers and for [Φ = 30°, K_r = 1, B = 0.2, E = 0.9, AR = 1 and D_1 = D_2 = 0.1]. It is clear that, as (Ra_m) values increase from [Ra_m = 150] to [Ra_m = 1000], the convection heat transfer in porous media and the strength of the fluid vortices are also increased. This can be seen from the maximum absolute values of the stream function which increase from [$|\Psi|_{,max}$ = 1.30] at [Ra_m=150] to [$|\Psi|_{,max}$ = 3.24] at [Ra_m=1000]. The effect of both the buoyancy force and the free convection in the porous media become very strong for high value of (Ra_m) which results in increasing the stream function values.With respect to isotherms, it is observed from Figure 12 that, when (Ra_m) is low [Ra_m=150], the isotherms are generally uniform. This is because of the significant influence of the conduction heat transfer. While for [Ra_m=1000], the convection inside the cavity is dominating, and the shape of the isotherms is obviously modified. The isotherms shape is changed from semi-curved pattern to the non- uniform curved pattern in the porous media. Also, isotherms distribution is almost uniform in the upper section of the left sidewall where the heat source locates for all the considered values of (Ra_m).

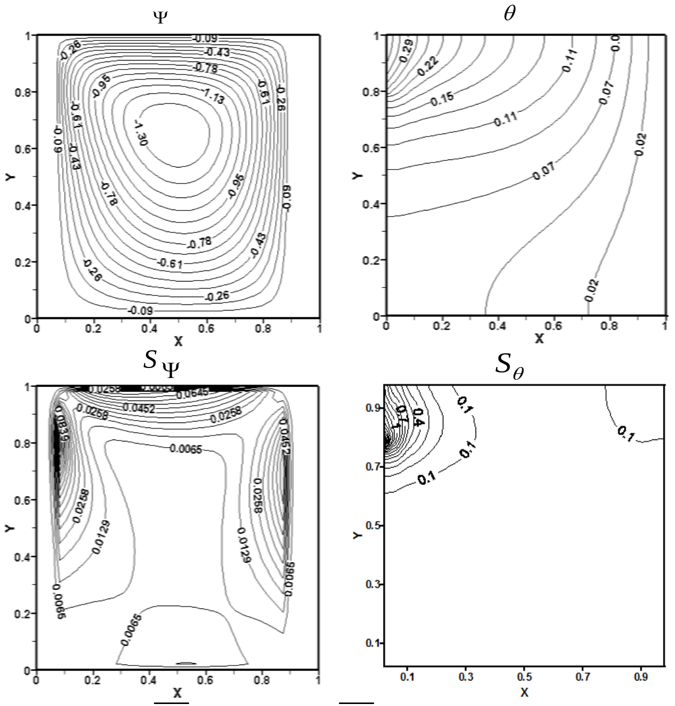

$\overline{Nu}_f = 0.22903, \overline{Nu}_s = 4.01883$

(a) $Ra_m = 150$

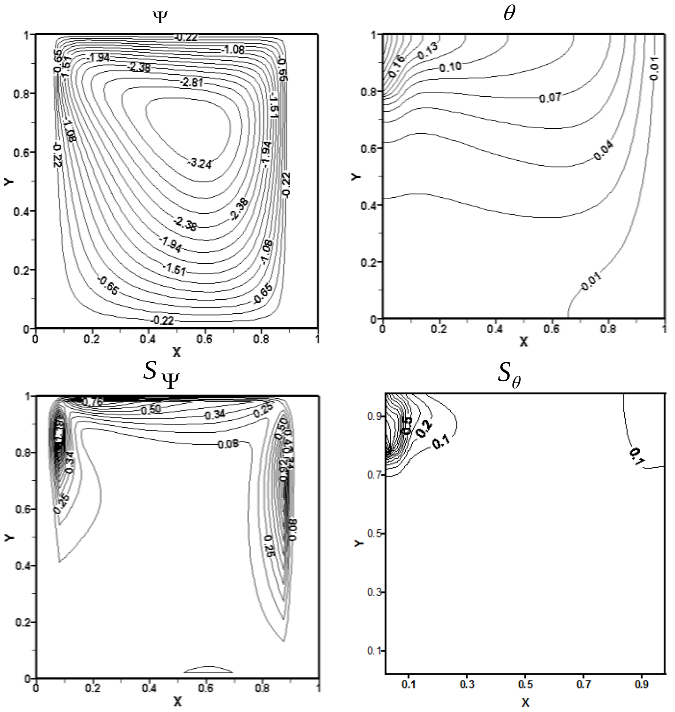

$\overline{Nu}_f = 0.22935, \overline{Nu}_s = 6.04888$

(b) $Ra_m = 1000$

Fig. 12. Streamlines contours (Ψ), isotherms contours (θ) and local entropy generated from fluid friction (S_Ψ) and heat transfer (S_θ) for various (Ra_m) and [B= 0.2, $D_1 = D_2 = 0.1$, $K_r = 1$, AR = 1, Φ = 30° and E = 0.9]

With respect to the local entropy generated from fluid friction and heat transfer, it may be noticed that as (Ra_m) values increase from [Ra_m = 150] to [Ra_m = 1000], a significant effect of the friction between the fluid flow and the walls was observed. This may be noticed from the maximum values of (S_Ψ) which increase respectively from [$S_{\Psi,max}$= 0.0839] to [$S_{\Psi,max}$ = 1.18] at the upper section of the left sidewall on the solid wall-fluid interfacial. Again, it can be seen an insignificant effect of (S_Ψ) in the center and the lower section of the cavity. This is caused by the weak effect of the friction between the fluid and the walls which resulted in reducing (S_Ψ) at these regions. For the entropy generated from the heat transfer, it may be noticed that these contours are accumulated at the upper section of the left sidewall where the heat source is positioned. This is because of the high heat transfer at this region which results an increasing (S_θ) at this location. For flow regions far from the heat source location especially within the porous media, the influence of (S_θ) becomes insignificant due to the weak effect of the heat source.

Figure 13 illustrates streamlines contours (Ψ), isotherms contours (θ) and local entropy generated from fluid friction (S_Ψ) and heat transfer (S_θ) for different heat source lengths and [Φ = 30°, K_r = 1, Ra_m = 1000, AR = 1 and D_1 = D_2 = 0.1]. For all values of the heat source length, the intensity of the fluid flow increases when the heat source length increases. This may be noticed from the maximum magnitudes of the stream function that increased from [$|\Psi|_{max}$ = 4.4] for [B = 0.4] to [$|\Psi|_{max}$ = 5.35] for [B = 0.6]. So, it may be concluded that the convection mode of the porous media is enhanced with the increase in the heat source length. It is also noticed that, the distribution of the isotherms is a strong function of the heat source length. It should be noted that, a big portion of the heat transfer from the heat source on the upper section of the left sidewall is transferred to the right cold sidewall due to the high temperature difference.

With respect to the behavior of the local entropy generated from fluid friction and heat transfer, Figure 13 shows that as the heat source length increases, the entropy generated from fluid friction becomes more pronounced especially at the interface regions. This is can be observed from the values of (S_Ψ) at the left wall-fluid interface region which increase from [$S_{\Psi,max.}$= 2.170] for [B = 0.4] to [$S_{\Psi,max.}$ = 3.109] for [B = 0.6]. This means that, the friction increases between the cavity walls and the fluid vortices at this region as heat source length increases. While, a weak effect of the friction between the wall and fluid vortices is noticed at the lower horizontal wall. Also, the effect of (S_Ψ) becomes slight at the central area of the cavity due to the low friction between the molecules of the fluid at this region. Figure 13 also shows that, the entropy generated from the heat transfer is a strong function of the heat source length. This can be seen from the distribution of (S_θ) close to the heat source location with the increase of the heat source length. While, a weak effect of (S_θ) is observed in the other regions of the cavity.

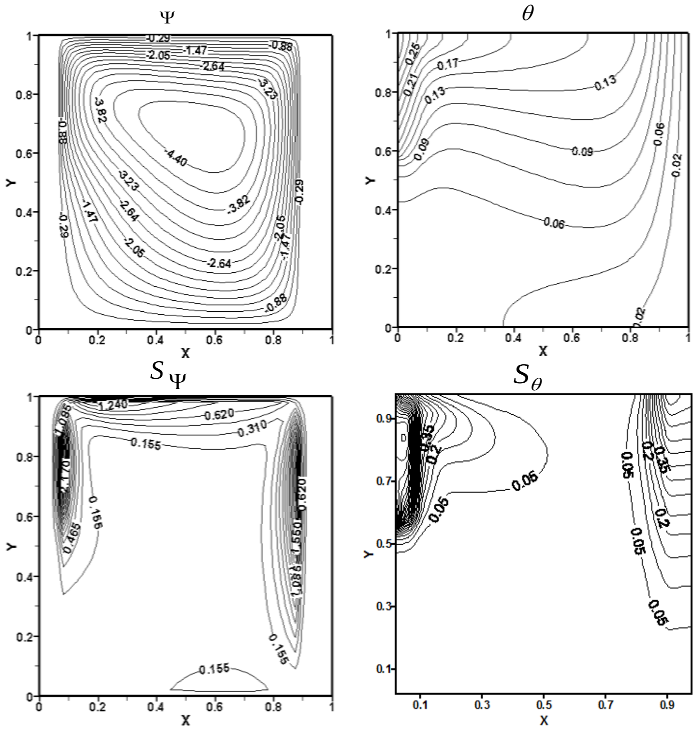

$\overline{Nu_f} = 0.41109, \overline{Nu_s} = 4.44547$

(a) B = 0.4

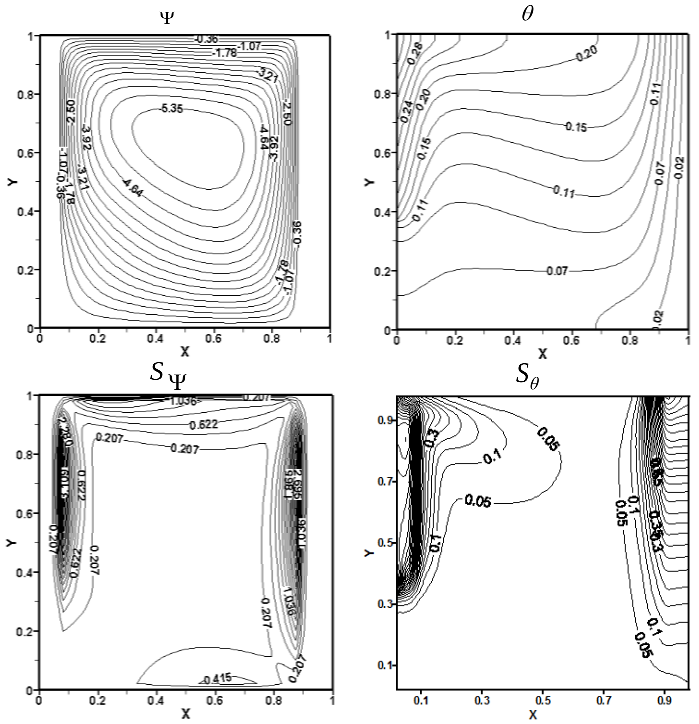

$\overline{Nu_f} = 0.63172, \overline{Nu_s} = 3.96262$

(b) B = 0.6

Fig. 13. Streamlines contours (Ψ), isotherms contours (θ) and local entropy generated from fluid friction (S_Ψ) and heat transfer (S_θ) for various heat source length and for [Φ = 30°, $D_1 = D_2 = 0.1$, $K_r = 1$, AR = 1, $Ra_m = 1000$ and E = 0.7]

Figure 14 presents streamlines contours (Ψ), isotherms contours (θ) and local entropy generated from fluid friction (S_Ψ) and heat transfer (S_θ) for various values of walls thickness and [Φ = 30°, AR = 1, Ra_m = 1000, E = 0.9, B = 0.2 and K_r = 1]. It was noticed that, at high values of walls thickness, the fluid vortices are low because of the convection reduction. In this case, where the wall thickness is increased the conduction is dominating. Note that, the maximum absolute values of the stream function decrease from [$|\Psi|_{max}$ = 2.99] for [$D_1 = D_2 = 0.15$] to [$|\Psi|_{max}$ = 2.81] for [$D_1 = D_2 = 0.2$] respectively. From the other hand, due to the significant effect of the conduction when the dimensionless walls thickness increases, it can be noticed that the isotherm contours become more uniform. With respect to the local entropy generated from fluid friction and heat transfer, it was noted that the effect of (S_Ψ) is dominant close to the cavity walls except the lower section and the central area of the cavity due to the low velocity gradient. Note that, at the left wall-fluid interfacial, the maximum magnitude of (S_Ψ) equals to [1.05] and [0.934] for cases [$D_1 = D_2 = 0.15$ and 0.2] respectively.The right sidewall and the top horizontal wall also represent another active zone of (S_Ψ), but with lower values when compared with that at the left wall-fluid interface region. In regards to the entropy generated from heat transfer; it is observed that they are accumulated at the upper left corner of the cavity where the heat source is positioned due to the high temperature gradient at this region.

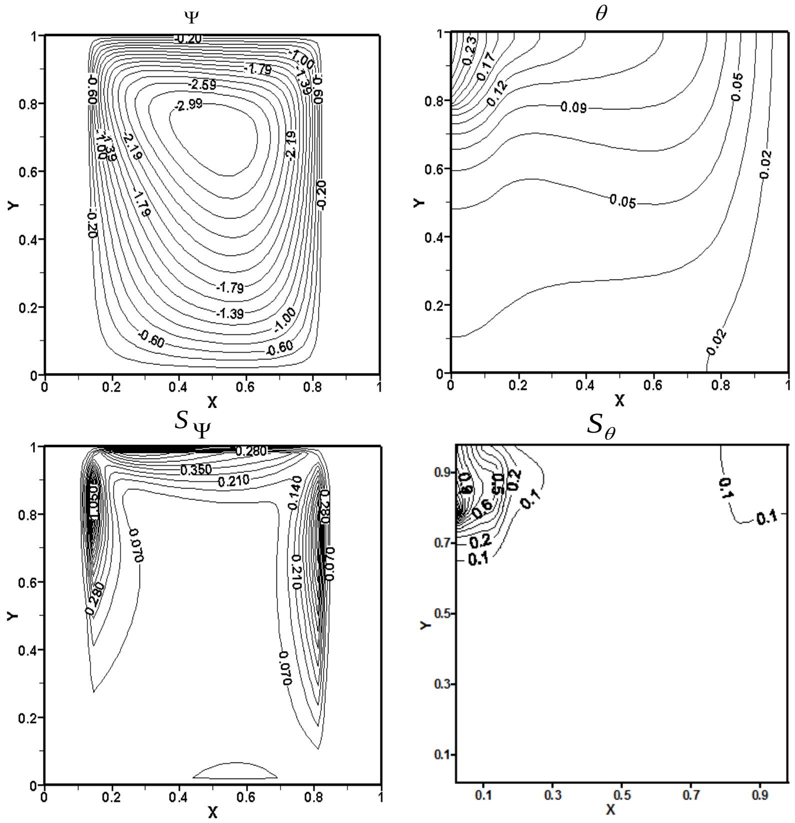

$\overline{Nu_f} = 0.22722, \overline{Nu_s} = 5.27210$

(a) $D_1 = D_2 = 0.15$

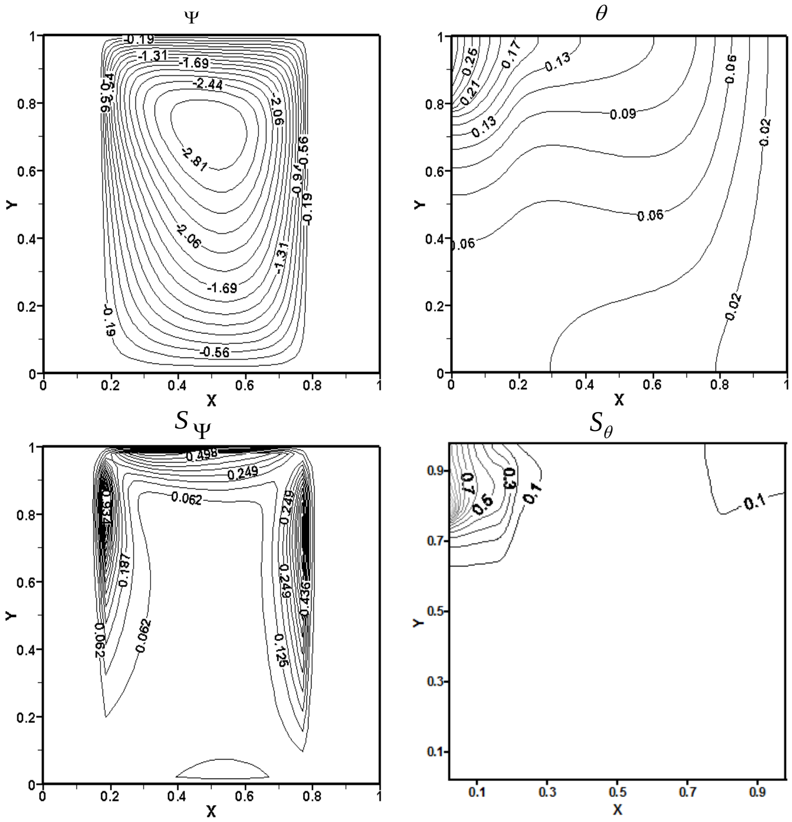

$\overline{Nu_f} = 0.22509, \overline{Nu_s} = 4.52072$

(b) $D_1 = D_2 = 0.2$

Fig. 14. Streamlines contours (Ψ), isotherms contours (θ) and local entropy generated from fluid friction (S_Ψ) and heat transfer (S_θ) for various dimensionless walls thickness and [B= 0.2, K_r = 1, Ra_m = 1000, AR = 1, Φ = 30°, E = 0.9]

3.3.2 Local Nusselt number results

The contours of (Nu_s) and (Nu_f) for various values of (Ra_m) and [B = 0.2, E= 0.9, K_r=1, D_1= D_2 = 0.1, AR=1 and Φ = 30°] are shown in Figure 15. From this figure, it may be noticed that, both (Nu_s) and (Nu_f) are increased as (Ra_m) increases. This is due to the enhanced convection and the buoyancy force in the porous cavity. With respect to behavior of (Nu_f), it can be observed that when (Ra_m) increases from [150] to [1000], the (Nu_f) values increase at the upper part of the left sidewall (i.e., at the heat source location). Whereas, an opposite behavior is noticed at the other parts of the left sidewall. This is due to the increase in the intensity of the convection currents which caused a clear change in the heat transfer. The influence of the heat source length on (Nu_s) and (Nu_f) profiles are illustrated in Figure 16 when [K_r = 1, Ra_m = 1000, D_1= D_2 = 0.1, AR = 1 and Φ = 30°]. It is clear that, (Nu_s) is in an inverse proportion to the heat source length for the same reason explained previously in case (1). With respect to (Nu_f) profiles, from Figure 16, it could be deduced that it is directly proportional to the heat source length. This can be seen from the behavior of (Nu_f) which was increased at the heat source location and then begins to decrease far away from it. Figure 17 shows the (Nu_s) and (Nu_f) for different values of the dimensionless walls thickness and for [B = 0.2, E = 0.9, Ra_m = 1000, K_r = 1, AR=1 and Φ = 30°]. It was noticed that, as the dimensionless wall thickness increases, the (Nu_s) profiles decrease. Since, the conductive walls become thicker and lead to reduce (Nu_s) values. From the opposite side, it can be seen from this figure, that the (Nu_f) near the middle section of the left sidewall, increases as the dimensionless walls thickness increase. Whereas, an opposite behavior is observed at the upper portions of the left sidewall. Since, the temperature differences between the interfacial and the cold boundary was reduced, as the dimensionless walls thickness increased, which reduces (Nu_f) at the upper portions of the left sidewall.

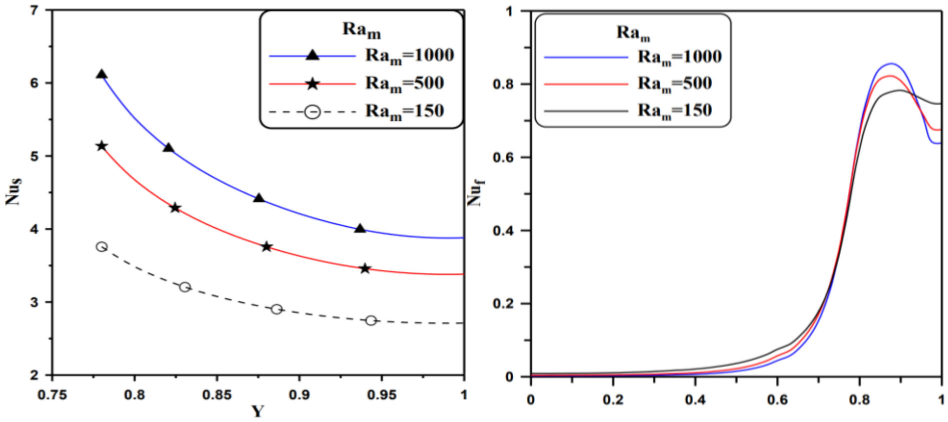

Nu_s Nu_f

Fig. 15. (Nu_s) and (Nu_f) contours for various values of (Ra_m) and for [B= 0.2, AR= 1, Φ= 30°, K_r= 1, D_1= D_2= 0.1 and E= 0.9]

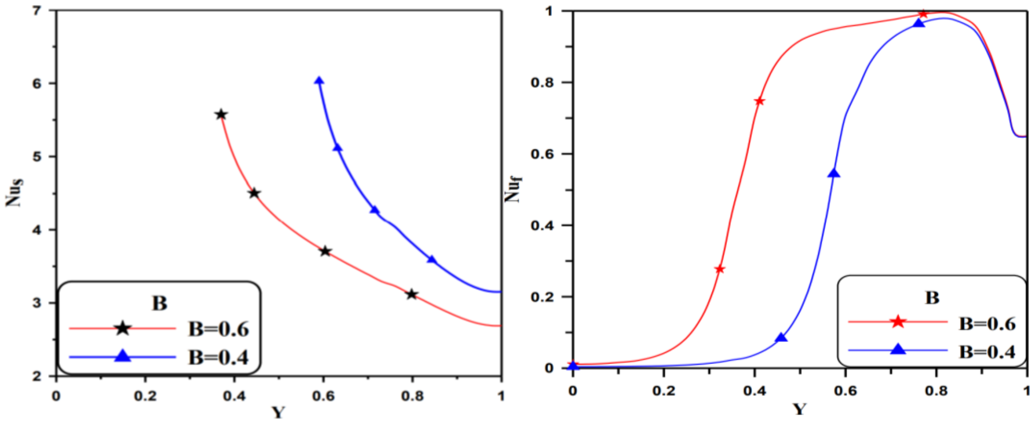

Nu_s Nu_f

Fig. 16. Profiles of (Nu_s) and (Nu_f) for various values of (B) and [Φ = 30°, D_1= D_2 = 0.1, AR= 1, Ra_m= 1000 and K_r= 1]

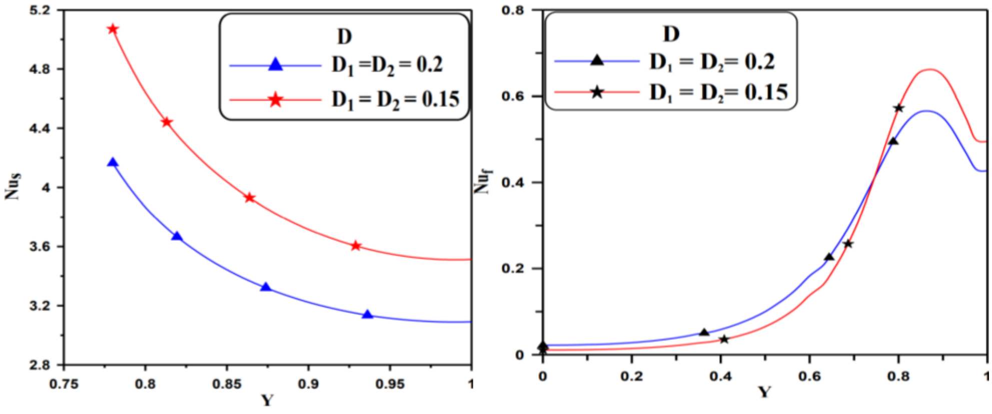

Nu_s Nu_f

Fig. 17. Profiles of (Nu_s) and (Nu_f) for various values of (D) and [B= 0.2, AR= 1, Φ= 30°, K_r= 1, Ra_m= 1000 and E= 0.9]

3.3.3 Average Nusselt number results

The results show that, ($\overline{Nu_s}$) increases with increasing (Ra_m and AR), while it decreases when (B and (D_1 and D_2)) increase. In regards to the behavior of ($\overline{Nu_f}$), it was noticed that it increases when (Ra_m and B) increase, whereas an opposite behavior of ($\overline{Nu_f}$) is observed when the walls thickness increases.

3.3.4 Average Bejan number results

The relation between the average Bejan number (Ba_{av}) and (Ra_m) for various values of the considered parameters for case (2) is presented in Figure 18. The results indicated that, as (Ra_m) increases, the (Ba_{av}) decreases for the entire range of considered values of the heat source length. It was also noted, that the (Ba_{av}) increases when (B) increases. In this case, the entropy generated from heat transfer was dominant. This can be seen from the minimum value of (Ba_{av}) which is greater than (0.5) as shown from Figure 18.

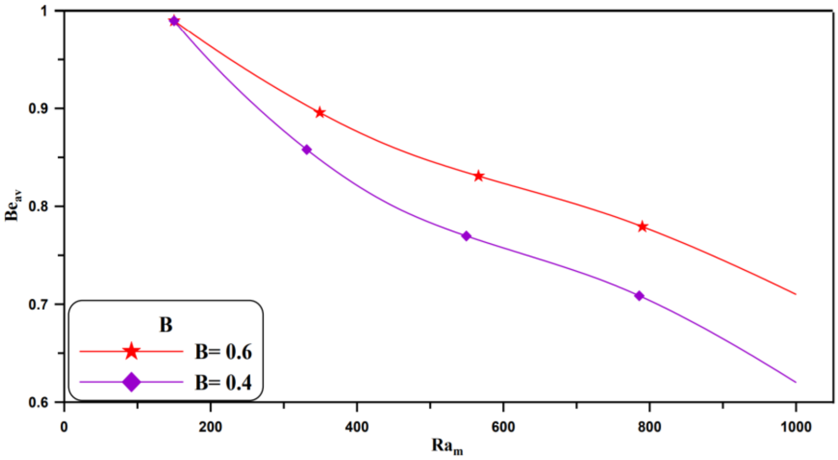

Fig. 18. Be_{av} versus (Ra_m) for various values of B and [K_r= 1, AR=1, Φ=30°, D_1=D_2=0.1, E=0.9]

3.4 Case Three

3.4.1 Streamlines, isotherms, and entropy generation results

Figure 19 displays streamlines contours (Ψ), isotherms contours (θ) and local entropy generated from fluid friction (S_Ψ) and heat transfer (S_θ) for different (Ra_m) and [Φ=30°, K_r=1, B=0.2, E=0.9, AR=1 and D_1=D_2=0.1]. As presented in Figure 19(a) for [Ra_m=150], the conduction heat transfer was dominating, but when (Ra_m) increases to [1000] the intensity of the fluid flow increases also. This may be noticed from the maximum value of the stream function that increases from [$\Psi_{,max}$=1.45] at [Ra_m=150] to [$\Psi_{,max}$ = 4.03] at [Ra_m=1000]. This means that, the convectionis enhanced for higher values of the modified-Rayleigh number [Ra_m=1000]. In regards to isotherms, it is clear from Figure 19 that for low (Ra_m) [Ra_m=150], the isotherms are in general have a uniform shape. But when (Ra_m) is high [Ra_m=1000], a distinct change in the isotherms shape is observed. This indicates that for low values of modified-Rayleigh number [Ra_m=150], conduction heat transfer is dominant, while for high (Ra_m) [i.e., Ra_m=1000], the convection is dominating. For the local entropy generated from fluid friction and heat transfer, it was noted that by increasing (Ra_m) from [Ra_m=150] to [Ra_m=1000], the fluid circulation strength becomes stronger and due to this phenomenon, the friction between the fluid's molecules and the walls increases also. Therefore, the maximum values of (S_{Ψ}) increase respectively from [S_{Ψ},max=0.125] to [S_{Ψ},max=1.63] at the lower section of the cavity. The other active zone of (S_{Ψ}) are also observed close to the middle section of the right sidewall and upper horizontal wall. Also, it can be noted that the effect of (Ra_m) on (S_{Ψ}) is weak at the left sidewall and the central area of the cavity. For (S_{θ}) contours, it may be noticed that, it is accumulated at the lower right corner of the cavity where the heat source locates. This is caused by the high temperature gradient at this region of the cavity which leads to high rates of heat transfer and consequently entropy generation. Also, weak effect of (S_{θ}) with the fluid phase and the top horizontal wall is observed due to the low temperature gradient. Figure 20 Illustrates streamlines contours (Ψ), isotherms contours (θ) and local entropy generated from fluid friction (S_{Ψ}) and heat transfer (S_{θ}) for various (K_r) and [Φ=30°, AR= 1, Ra_m= 1000, E= 0.9, B= 0.2 and $D_1 = D_2 = 0.1$]. It was noticed that, with increasing (K_r), the resistance of the solid walls reduces and then the convection impact in the fluid becomes stronger. Thus, the values of the stream function increase from [Ψ,max= 8.23] for [$K_r = 5$] to [Ψ,max = 10.95] for [$K_r = 10$] respectively. Therefore, it may be deduced that the free convection increases as (K_r) values increase. With respect to isotherms, it was noticed that as values of (K_r) increase from [$K_r = 5$] to [$K_r = 10$], the isotherms distribution is adjacent to the lower (heated part) and upper (cold part) right interface regions between the fluid and the walls. This is caused by the increment of the temperature gradient which is resulted from the increase of (K_r).For the behavior of both the local entropy generated from fluid friction and heat transfer, it was noticed that when (K_r) increases, the values of (S_{Ψ}) increases especially at the interface regions between the fluid and the walls due to same reasons explained above. Also, the right sidewall represents an active place of (S_{Ψ}), but with slow increasing values as (K_r) increases. From Figure 20, it can be observed also that, the effect of (S_{Ψ}) is weak at the central area of the cavity and the left sidewall for all values of (K_r) because of low fluid friction at these regions. With respect to (S_{θ}), it can be noted that they are accumulated close to the interface regions between the fluid and the cavity walls for all values of (K_r). This is caused by high temperature gradient that resulted in magnifying the heat transfer rate, and consequently the values of (S_{θ}) are increased.

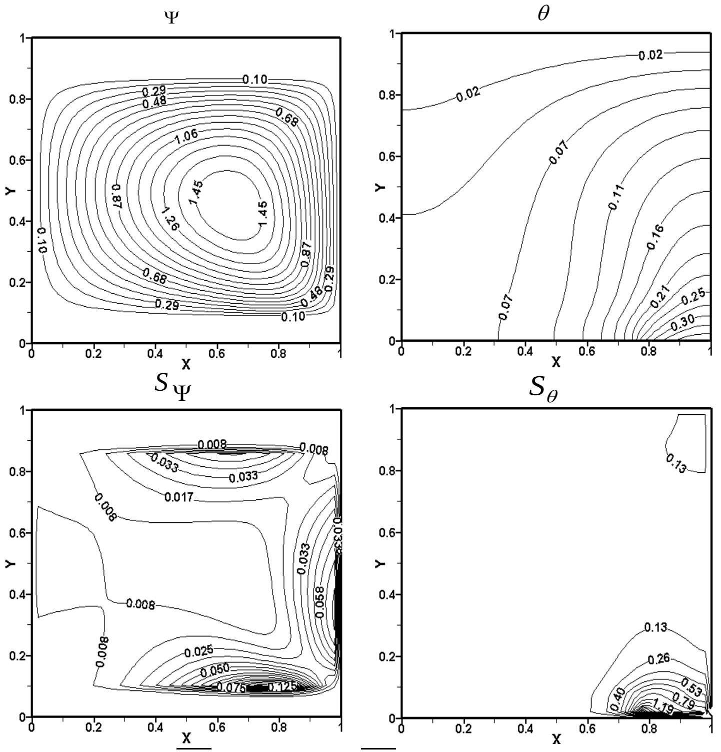

$\overline{Nu_f} = 0.23092, \overline{Nu_s} = 2.26609$

(a) $Ra_m = 150$

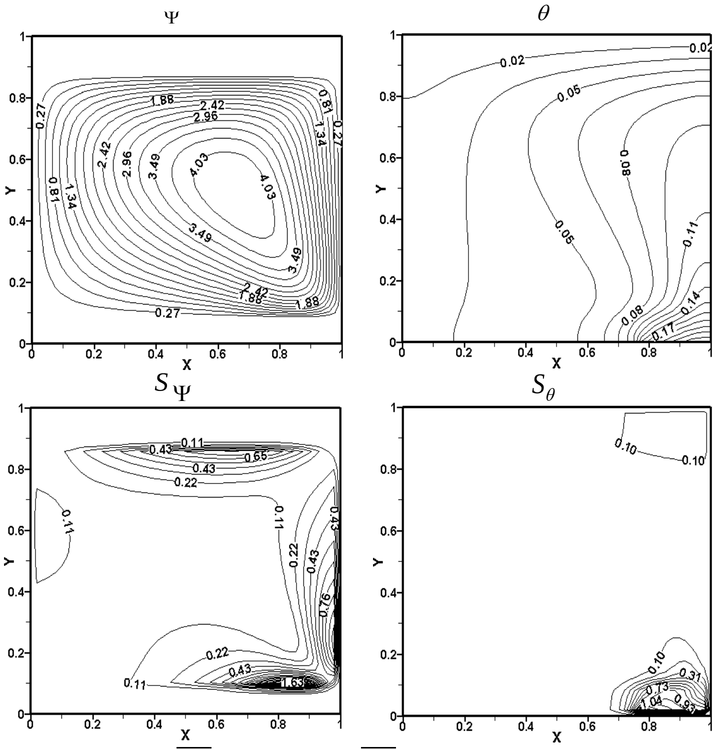

$\overline{Nu_f} = 0.23164, \overline{Nu_s} = 3.60526$

(b) $Ra_m = 1000$

Fig. 19. Streamlines contours (Ψ), isotherms contours (θ) and local entropy generated from fluid friction (S_Ψ) and heat transfer (S_θ) for various (Ra_m) and [B = 0.2, $D_1 = D_2$ = 0.1, K_r = 1, AR = 1, Φ = 30°, E = 0.9]

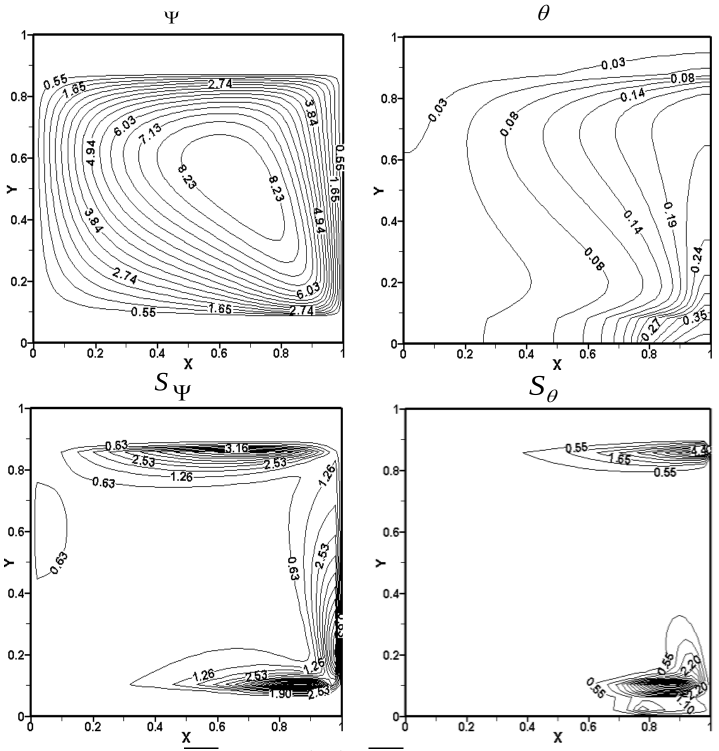

$\overline{Nu_f} = 1.15252, \overline{Nu_s} = 2.4006$

(a) $K_r = 5$

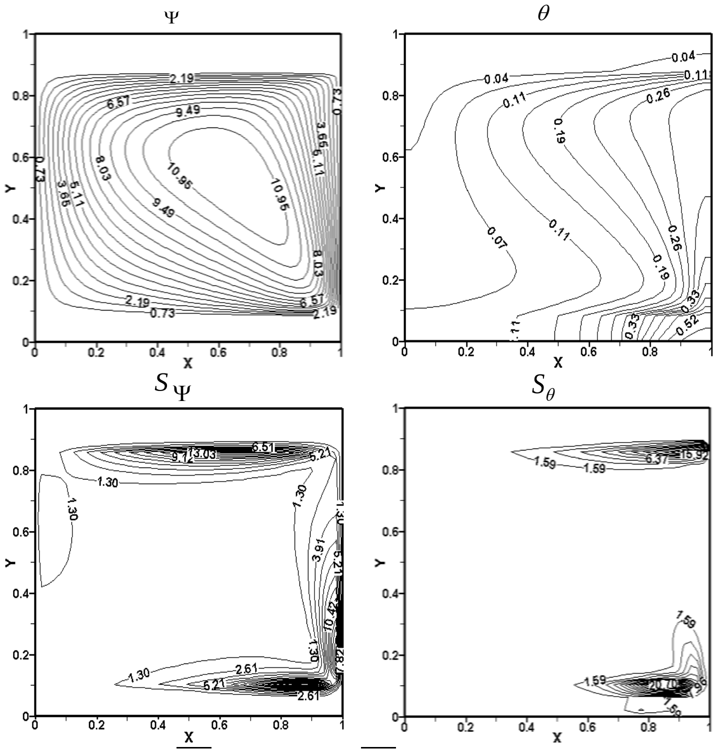

$\overline{Nu_f} = 2.32179, \overline{Nu_s} = 1.98175$

(b) $K_r = 10$

Fig. 20. Streamlines contours (Ψ), isotherms contours (θ) and local entropy generated from fluid friction (S_Ψ) and heat transfer (S_θ) for various values of (K_r) and [B= 0.2, D_1 = D_2 = 0.1, Ra_m = 1000, AR = 1, Φ = 30°, E = 0.9]

Figure 21 illustrates streamlines contours (Ψ), isotherms contours (θ) and the local entropy generated from fluid friction (S_Ψ) and heat transfer (S_θ) for various values of walls thickness and [Φ = 30°, AR = 1, Ra_m = 1000, E = 0.9, B = 0.2 and K_r = 1]. The flow circulation intensity for thin solid walls is considerably high. This is noticed from the reduction of the maximum values of the stream function from [Ψ = 4.03] for [$D_1 = D_2 = 0.15$] to [Ψ = 3.39] for [$D_1 = D_2 = 0.2$]. This demonstrates that, the conduction is dominating for high walls thickness. For isotherm contours, it may be observed that, they are agglomerated vicinity of the heat source position and turn out to be smoother as the dimensionless walls thickness increases for the same reason that mentioned above. With respect to the local entropy generated from fluid friction and heat transfer, it may be noticed that when the walls thickness is increased, the effect of (S_Ψ) is decreased due to lower flow circulation intensity. This is observed from the maximum values of (S_Ψ) that is decreased from [1.305] for [$D_1 = D_2 = 0.15$] to [1.12] for [$D_1 = D_2 = 0.2$] at the lower wall- fluid interface. Another active places of (S_Ψ) are at the right sidewall and top horizontal wall but with lower values when compared with that at the lower wall- fluid interface. While, a negligible effect of fluid friction can be noticed in the left sidewall. For the behavior of the entropy generated from heat transfer, since the conduction is dominating as the wall thickness is increased, the (S_θ) contours become smoother at the end of the lower wall where the heat source is placed.

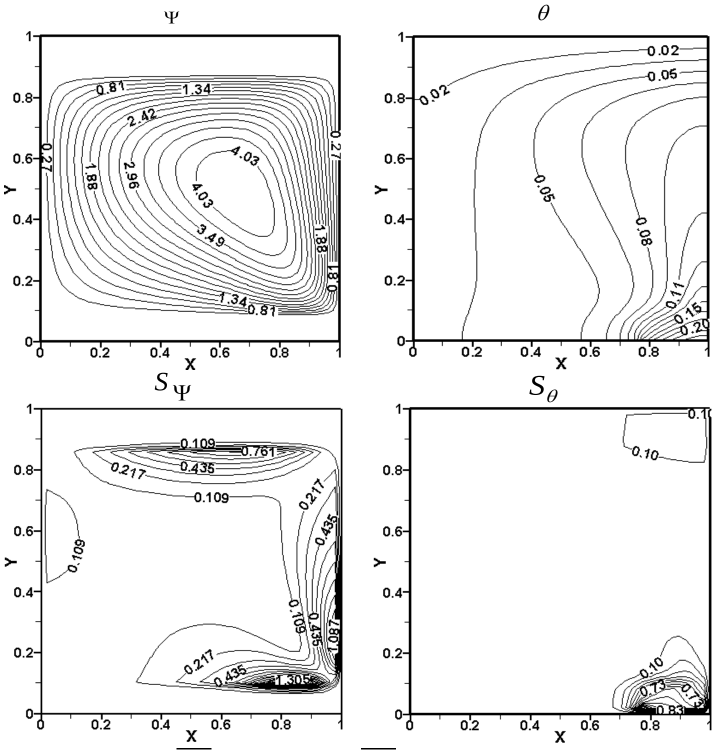

$\overline{Nu}_f = 0.23164, \overline{Nu}_s = 3.60526$

(a) $D_1 = D_2 = 0.15$

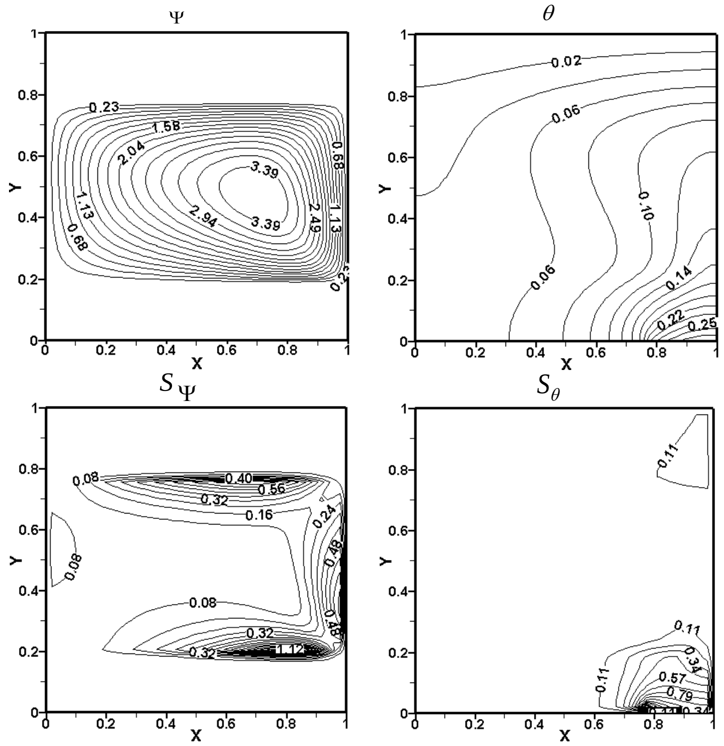

$\overline{Nu_f} = 2.32179, \overline{Nu_s} = 1.98175$

(b) $D_1 = D_2 = 0.2$

Fig. 21. Streamlines contours (Ψ), isotherms contours (θ) and local entropy generated from fluid friction (S_Ψ) and heat transfer (S_θ) for various dimensionless walls thickness and [B= 0.2, K_r = 1, Ra_m = 1000, AR = 1, Φ = 30°, E = 0.9]

3.4.2 Local Nusselt number

The profiles of (Nu_s) and (Nu_f) for various values of (Ra_m) and [B = 0.2, E= 0.9, K_r=1, D_1=D_2 = 0.1, AR=1 and Φ = 30°] are displayed in Figure 22. The convection becomes more pronounced as (Ra_m) increases from [150] to [1000] due to the enhanced the buoyancy force over the viscous force. For this reason, both (Nu_s) and (Nu_f) profiles are increased also. For the behavior of (Nu_f) profiles, it may be observed that they increase with (Ra_m) at the heat source location, while a reverse behavior can be observed at mid region of bottom horizontal wall. Figure 23 presents the variation of (Nu_s) and (Nu_f) for various thermal conductivity ratios (K_r) and [B = 0.2, E= 0.9, Ra_m = 1000, D_1= D_2 = 0.1, AR = 1 and Φ = 30°]. The results show that, the profiles of (Nu_s) decrease as (K_r) increases, while (Nu_f) increases as (K_r) increases. Figure 24 shows the (Nu_s) (left) and (Nu_f) (right) for different values of the dimensionless walls thickness and [B = 0.2, E= 0.9, Ra_m = 1000, K_r = 1, AR=1 and Φ = 30°]. As shown in this figure that, the (Nu_s) decreases with increasing walls thickness. Since, the conduction begins dominant as the walls thickness increases. With respect to the profile of (Nu_f), it can be seen that, it decreases at the end portion of the lower horizontal wall when values of walls thickness increase. Whereas, an opposite behavior of (Nu_f) profiles is noticed at the other parts of the same wall.

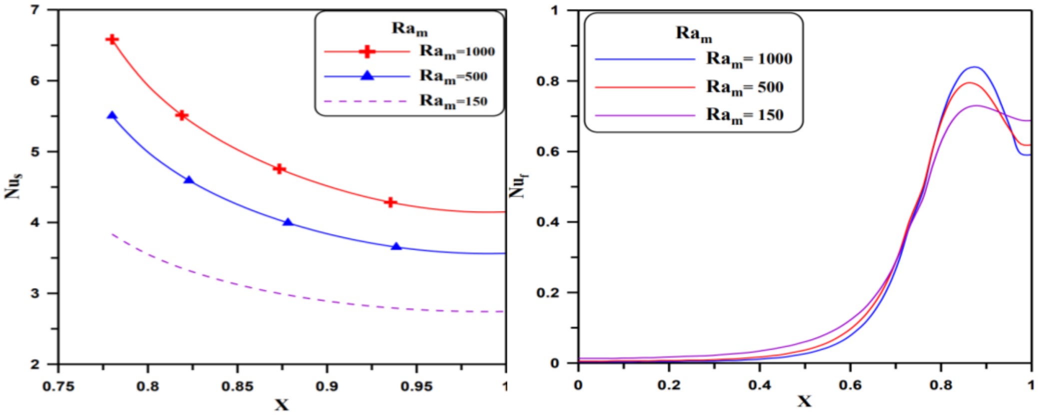

Nuf Nus

Fig. 22. Profiles of (Nuf) and (Nus) for different values of (Ram) and [B= 0.2, AR= 1, Φ= 30°, Kr= 1, D1= D2= 0.1 and E= 0.9]

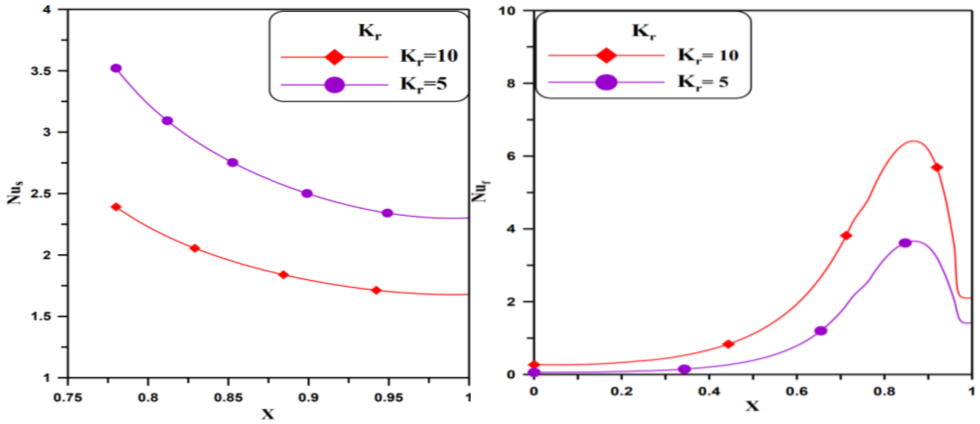

Nuf Nus

Fig. 23. Profiles of (Nuf) and (Nus) for different values of (Kr) and [B= 0.2, AR= 1, Φ= 30°, Ram= 1000, D1= D2= 0.1 and E= 0.9]

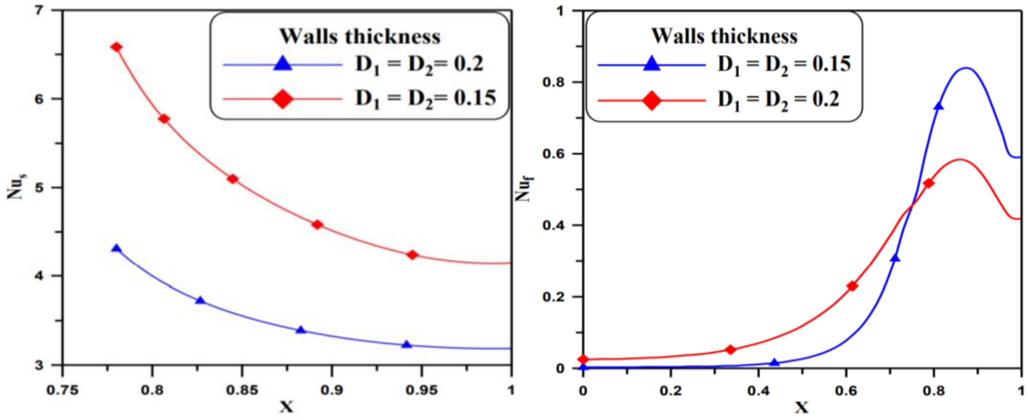

Nuf Nus

Fig. 24. Profiles of (Nub) and (Nus) for different values of equal walls thickness and [B = 0.2, AR = 1, Φ = 30°, Kr = 1, Ram = 1000 and E = 0.9]

3.4.3 Average Nusselt number results

In regards to the average Nusselt number behaviour along the heat source, it may be observed that it increases with increasing (Ra_m), while it decreases when (K_r, D_1 and D_2) increase.

For the behavior of ($\overline{Nu_f}$), it can be seen that it increases when (Ra_m) and (K_r) increase, while a reverse behavior of ($\overline{Nu_f}$) is observed when (D_1) and (D_2) increase.

3.4.4 Average Bejan number results

Figure 25 and Figure 26 present the profiles of the average (Be_{av}) versus (Ra_m) for various values of the considered parameters for case (3). The results indicate that, the values of (Be_{av}) are decreased as (Ra_m) is increased from [Ra_m= 150] to [Ra_m = 1000]. This is due to increase the intensity of the fluid circulations. For lower value of (Ra_m) (i.e., Ra_m = 150), the entropy generated from heat transfer is dominating, while the entropy generated from fluid friction begins to dominate with the increase of (Ra_m). From these figures, it was noticed that (Be_{av}) is decreased with increasing (K_r and (D_1 and D_2)). For this case, the entropy generated from fluid friction is dominating, this may be noticed from the values of (Be_{av}) which are lower than (0.5) for [Ra_m = 1000].

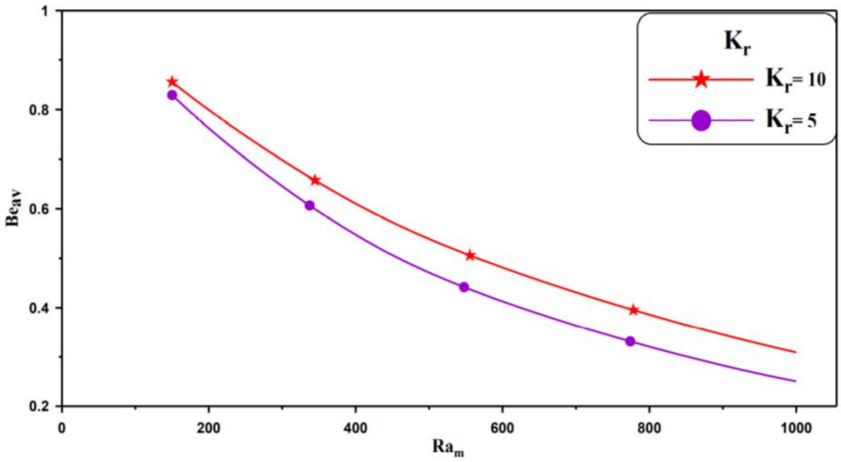

Fig. 25. Average Bejan number (Be_{av}) versus (Ra_m) for different values of (K_r) and [B= 0.2, AR= 1, Φ= 30°, Ra_m= 1000, D_1= D_2= 0.1 and E= 0.9]

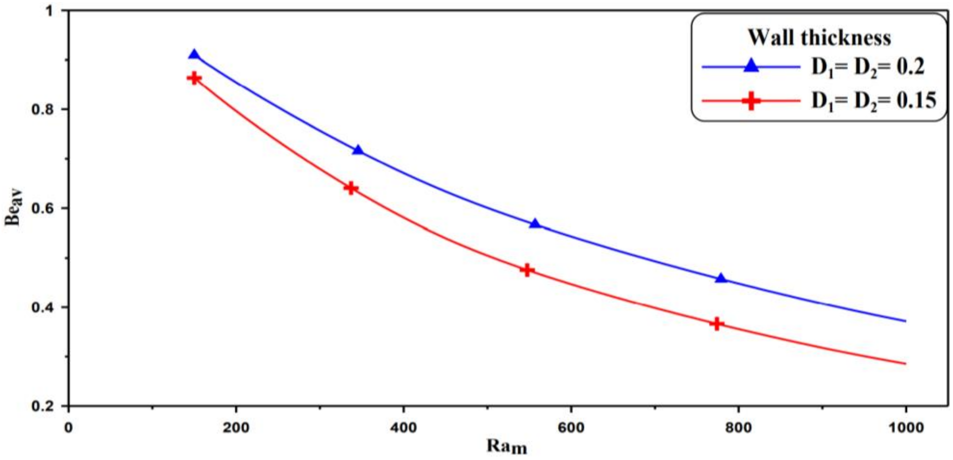

Fig. 26. Average Bejan number (Be_{av}) versus (Ra_m) for different values of equal walls thickness (D_1 and D_2) and [B= 0.2, AR= 1, Φ= 30°, K_r= 1, Ra_m= 1000 and E=0.9]

4. Conclusions

The present work deals with the numerical simulation of the entropy production of the conjugate natural convection in a tilted porous cavity with respect to heat source and solid wall's locations. It was found that, the strength of the fluid flow and the convection heat transfer are directly proportional to (Ra_m), (K_r), (B) and (AR). While, they are inversely proportional to cavity walls thickness. For all considered cases, the isotherm lines tend to be more curved as (Ra_m), (K_r), (B) and (AR) increased. While, an opposed behavior is noted when the walls thickness increased. Both the average and local Nusselt numbers of the fluid increase, when (K_r) and (B) increase, while, an opposite behavior is found with respect to the local and average Nusselt numbers along the heat source. This behavior was observed for all considered cases. Also, the local and average Nusselt numbers of the fluid and along the heat source are directly proportional to (Ra_m). From the other hand, the local Nusselt number of the fluid phase near the middle section of wall is directly proportional to the dimensionless walls thickness. Whereas, an opposite behavior of it was noticed at the heat source location. This behavior was observed also for all considered cases. The maximum values of the entropy generated from fluid friction are located close to the cavity wall-fluid interfacial, while the maximum values of the entropy generated from the heat transfer occur near the heat source region. But, the influence of entropy generated from heat transfer and fluid friction is insignificant at the cavity central zone. The average Bejan number is higher than (0.5) for both cases one and two, while for case three, it was found to be less than (0.5), for all considered parameters. Finally, it was concluded that, the maximum heat transfer rate was achieved in case three. For this case, the maximum value of the stream function was enhanced by about (36 %) with increasing (Ra_m). While, the maximum values of (S_Ψ) was increased by about (8 %).

Acknowledgments

This publication was supported by the Deanship of Scientific Research at Prince Sattam bin Abdulaziz University, Alkharj, Saudi Arabia.

References

[1] Pop, Ioan, and Derek B. Ingham. *Convective heat transfer: mathematical and computational modelling of viscous fluids and porous media*. Elsevier, 2001.

[2] Vafai, Kambiz, ed. *Handbook of Porous Media*. CRC Press, 2005. https://doi.org/10.1201/9780415876384

[3] Ingham, Derek B., and Ioan Pop, eds. *Transport phenomena in porous media III*. Vol. 3. Elsevier, 2005.

[4] Nield, Donald A., and Adrian Bejan. *Convection in porous media*. Vol. 3. New York: springer, 2006.

[5] Basak, Tanmay, S. Roy, T. Paul, and I. Pop. "Natural convection in a square cavity filled with a porous medium: effects of various thermal boundary conditions." *International Journal of Heat and Mass Transfer* 49, no. 7-8 (2006): 1430-1441. https://doi.org/10.1016/j.ijheatmasstransfer.2005.09.018

[6] Revnic, C., I. Pop, T. Grosan, and D. B. Ingham. "Natural convection in an inclined square cavity with heated and cooled adjacent walls and filled with a porous medium." *The Open Conservation Biology Journal* 1, no. 1 (2009): 20-29. https://doi.org/10.2174/1877729500901010020

[7] Sheikhzadeh, G. A., and S. Nazari. "Numerical study of natural convection in a square cavity filled with a porous medium saturated with nanofluid."*Transport Phenomena in Nano and Micro Scales* 1 (2013): 138-146.

[8] Khansila, Paweena, and Supot Witayangkurn. "Visualization of natural convection in enclosure filled with porous medium by sinusoidally temperature on the one side." *Applied Mathematical Sciences* 6, no. 97 (2012): 4801-4812.

[9] Selamat, Mat Salim, Rozaini Roslan, and Ishak Hashim. "Natural convection in an inclined porous cavity with spatial sidewall temperature variations." *Journal of Applied Mathematics* 2012 (2012). https://doi.org/10.1155/2012/939620

[10] Molla, Md Mamun, Suvash Saha, and M. A. I. Khan. "Natural convection flow in a porous enclosure with localized heating from below." *JP Journal of Heat and Mass Transfer* 6, no. 1 (2012): 1-16.

[11] Kalaoka, Wiratchada, and Supot Witayangkurn. "Natural convection in a porous square enclosure with partially cooled from vertical wall." *Current Applied Science and Technology* 12, no. 2 (2012): 180-188.
[12] Kalaoka, Wiratchada, and Supot Witayangkurn. "Natural convection in porous square cavities with discrete heat sources on bottom and side walls." *Thai Journal of Mathematics* 12, no. 1 (2013): 207-221.
[13] Saeid, Nawaf H. "Conjugate natural convection in a porous enclosure: effect of conduction in one of the vertical walls." *International Journal of Thermal Sciences* 46, no. 6 (2007): 531-539. https://doi.org/10.1016/j.ijthermalsci.2006.08.003
[14] Saeid, Nawaf H. "Conjugate natural convection in a vertical porous layer sandwiched by finite thickness walls." *International Communications in Heat and Mass Transfer* 34, no. 2 (2007): 210-216. https://doi.org/10.1016/j.icheatmasstransfer.2006.11.003
[15] Al-Amiri, Abdalla, Khalil Khanafer, and Ioan Pop. "Steady-state conjugate natural convection in a fluid-saturated porous cavity." *International Journal of Heat and Mass Transfer* 51, no. 17-18 (2008): 4260-4275. https://doi.org/10.1016/j.ijheatmasstransfer.2007.12.026
[16] Saleh, H., and Ishak Hashim. "Conjugate natural convection in a porous enclosure with non-uniform heat generation." *Transport in Porous Media* 94, no. 3 (2012): 759-774. https://doi.org/10.1007/s11242-012-0023-z
[17] Chamkha, Ali J., and Muneer A. Ismael. "Conjugate heat transfer in a porous cavity heated by a triangular thick wall." *Numerical Heat Transfer, Part A: Applications* 63, no. 2 (2013): 144-158. https://doi.org/10.1080/10407782.2012.724327
[18] Alhashash, A., H. Saleh, and I. Hashim. "Effect of conduction in bottom wall on Benard convection in a porous enclosure with localized heating and lateral cooling." *Transport in Porous Media* 96, no. 2 (2013): 305-318. https://doi.org/10.1007/s11242-012-0089-7
[19] Zahmatkesh, Iman. "Second-law analysis of buoyancy-driven flow inside a rectangular porous enclosure with three adiabatic walls." *Majlesi Journal of Energy Management* 1, no. 4 (2012): 15-22.
[20] Varol, Yasin, Hakan F. Oztop, and Ahmet Koca. "Entropy generation due to conjugate natural convection in enclosures bounded by vertical solid walls with different thicknesses." *International Communications in Heat and Mass Transfer* 35, no. 5 (2008): 648-656. https://doi.org/10.1016/j.icheatmasstransfer.2008.01.010
[21] Kaluri, Ram Satish, and Tanmay Basak. "Entropy generation due to natural convection in discretely heated porous square cavities." *Energy* 36, no. 8 (2011): 5065-5080. https://doi.org/10.1016/j.energy.2011.06.001
[22] Kaluri, Ram Satish, and Tanmay Basak. "Role of entropy generation on thermal management during natural convection in porous square cavities with distributed heat sources." *Chemical Engineering Science* 66, no. 10 (2011): 2124-2140. https://doi.org/10.1016/j.ces.2011.02.009
[23] Basak, Tanmay, Ram Satish Kaluri, and A. R. Balakrishnan. "Entropy generation during natural convection in a porous cavity: effect of thermal boundary conditions." *Numerical Heat Transfer, Part A: Applications* 62, no. 4 (2012): 336-364. https://doi.org/10.1080/10407782.2012.691059
[24] Basak, Tanmay, Abhishek Kumar Singh, Rini Richard, and S. Roy. "Finite element simulation with heatlines and entropy generation minimization during natural convection within porous tilted square cavities." *Industrial & Engineering Chemistry Research* 52, no. 23 (2013): 8046-8061. https://doi.org/10.1021/ie4005755
[25] Lam, Prasanth Anand Kumar, and K. Arul Prakash. "A numerical study on natural convection and entropy generation in a porous enclosure with heat sources." *International Journal of Heat and Mass Transfer* 69 (2014): 390-407. https://doi.org/10.1016/j.ijheatmasstransfer.2013.10.009
[26] Basak, Tanmay, Abhishek Kumar Singh, and R. Anandalakshmi. "Analysis of entropy generation during conjugate natural convection within a square cavity with various location of wall thickness." *Industrial & Engineering Chemistry Research* 53, no. 9 (2014): 3702-3722. https://doi.org/10.1021/ie403033f
[27] Zahmatkesh, Iman. "Dependence of buoyancydriven flow inside an oblique porous cavity on its orientation." *Emirates Journal for Engineering Research* 18, no. 2 (2013): 53-61.
[28] Japar, Wan Mohd Arif Aziz, Nor Azwadi Che Sidik, and Yutaka Asako. "Entropy generation minimization in sinusoidal cavities-ribs microchannel heat sink via secondary channel geometry." *CFD Letters* 11, no. 7 (2019): 1-10.
[29] Armaghani, T., Ali Chamkha, A. M. Rashad, and M. A. Mansour. "Inclined magneto: convection, internal heat, and entropy generation of nanofluid in an I-shaped cavity saturated with porous media." *Journal of Thermal Analysis and Calorimetry* 142, no. 6 (2020): 2273-2285. https://doi.org/10.1007/s10973-020-09449-6
[30] Yang, Kun, Wei Huang, Xin Li, and Jiabing Wang. "Analytical analysis of heat transfer and entropy generation in a tube filled with double-layer porous media." *Entropy* 22, no. 11 (2020): 1214. https://doi.org/10.3390/e22111214
[31] Dutta, Shantanu, Navneet Goswami, Sukumar Pati, and Arup Kumar Biswas. "Natural convection heat transfer and entropy generation in a porous rhombic enclosure: influence of non-uniform heating." *Journal of Thermal Analysis and Calorimetry* 144, no. 4 (2021): 1493-1515. https://doi.org/10.1007/s10973-020-09634-7
[32] Lukose, Leo, and Tanmay Basak. "Finite element-based evaluation on the role of various shaped containers (oil saturated porous media) for entropy generation versus heating efficiency involving thermal convection with

identical heating." *Numerical Heat Transfer, Part A: Applications* (2021): 1-80. https://doi.org/10.1080/10407782.2021.1884413

[33] Almuhtady, Ahmad, Muflih Alhazmi, Wael Al-Kouz, Zehba A. Raizah, and Sameh E. Ahmed. "Entropy Generation and MHD Convection within an Inclined Trapezoidal Heated by Triangular Fin and Filled by a Variable Porous Media." *Applied Sciences* 11, no. 4 (2021): 1951. https://doi.org/10.3390/app11041951

[34] Sheikholeslami, M., M. Jafaryar, Zafar Said, Ammar I. Alsabery, Houman Babazadeh, and Ahmad Shafee. "Modification for helical turbulator to augment heat transfer behavior of nanomaterial via numerical approach." *Applied Thermal Engineering* 182 (2021): 115935. https://doi.org/10.1016/j.applthermaleng.2020.115935

[35] Sheikholeslami, M., Seyyed Ali Farshad, and Zafar Said. "Analyzing entropy and thermal behavior of nanomaterial through solar collector involving new tapes." *International Communications in Heat and Mass Transfer* 123 (2021): 105190. https://doi.org/10.1016/j.icheatmasstransfer.2021.105190

[36] Mahdi, M. "Numerical Simulation of Entropy production for Conjugate Heat Transfer in a tilted Porous Cavity." *Master's Thesis, Babylon University, Iraq*, 2015.

[37] Aziz Japar , W., Che Sidik, N. and Beriache , M. "Hydrothermal performance in a new designed hybrid microchannel heat sink with optimum secondary channel geometry parameter : numerical and experimental studies." *Journal of Advanced Research Design* 54, no. 1 (2019): 13-27.